New Geophysical Technique for Mineral Exploration and Mineral Discrimination Based on Electromagnetic Methods

DE-FC26-04NT42081

FINAL REPORT

Principal Author: **Michael S. Zhdanov**
University of Utah, Salt Lake City, UT 84112

Reporting Period Start Date: April 9, 2004
Reporting Period End Date: April 9 2006

July 2006

Abstract

The research during the first two years of the project was focused on developing the foundations of a new geophysical technique for mineral exploration and mineral discrimination, based on electromagnetic (EM) methods. The developed new technique is based on examining the spectral induced polarization effects in electromagnetic data using effective-medium theory and advanced methods of 3-D modeling and inversion.

The analysis of IP phenomena is usually based on models with frequency dependent complex conductivity distribution. In this project, we have developed a rigorous physical/mathematical model of heterogeneous conductive media based on the effective-medium approach. The new generalized effective-medium theory of IP effect (GEMTIP) provides a unified mathematical method to study heterogeneity, multi-phase structure, and polarizability of rocks. The geoelectrical parameters of a new composite conductivity model are determined by the intrinsic petrophysical and geometrical characteristics of composite media: mineralization and/or fluid content of rocks, matrix composition, porosity, anisotropy, and polarizability of formations. The new GEMTIP model of multi-phase conductive media provides a quantitative tool for evaluation of the type of mineralization, and the volume content of different minerals using electromagnetic data.

We have developed a 3-D EM-IP modeling algorithm using the integral equation (IE) method. Our IE forward modeling software is based on the contraction IE method, which improves the convergence rate of the iterative solvers. This code can handle various types of sources and receivers to compute the effect of a complex resistivity model. We have demonstrated that the generalized effective-medium theory of induced polarization (GEMTIP) in combination with the IE forward modeling method can be used for rock-scale forward modeling from grain-scale parameters. The numerical modeling study clearly demonstrates how the various complex resistivity models manifest differently in the observed EM data. These modeling studies lay a background for future development of the IP inversion method, directed at determining the electrical conductivity and the intrinsic chargeability distributions, as well as the other parameters of the relaxation model simultaneously. The new technology introduced in this project can be used for the discrimination between uneconomic mineral deposits and the location of zones of economic mineralization and geothermal resources.

DISCLAIMER:

Contents

List of Figures

1. INTRODUCTION

This project was undertaken using multipartner collaboration between the University of Utah, four major mining companies, Kennecott Exploration Company located in Utah, USA; BHP Billiton World Exploration Inc. with offices in the USA, Canada, and Australia; Placer Dome Inc. with offices in Canada and the USA, Phelps Dodge Mining Company with offices in the USA and overseas, and Zonge Engineering and Research Organization, Inc. located in Tucson, Arizona, an equipment manufacturer and service provider to the mining industry.

The mineral industry needs a reliable method to distinguish between uneconomic mineral deposits and economic mineralization. The main goal of this project is to develop a new geophysical technique for subsurface material characterization, mineral exploration and mineral discrimination, based on electromagnetic (EM) methods. The developed new technique detects induced polarization (IP) effects in electromagnetic data and uses surface geophysical observations to determine the parameters of the conductivity relaxation model. These parameters are ultimately used for the discrimination of different types of rock formation.

It is a further object of this project to develop a new theoretical model and a method for quantitative interpretation of IP data in a complex 3-D environment. An important part of our project includes development of a new generalized effective medium theory of the IP effect (GEMTIP), which treats in a unified way different complex models of the multiphase composite models of the rocks. These new models and method can be used for examining the IP effect in complex rock formations with different mineral structures and electrical properties.

The new technology introduced in this project, can be used for interpretation of the ground, borehole, and airborne EM data. The recovered parameters of the relaxation model are used for the discrimination of different rocks, and in this way provide an ability to distinguish between uneconomic mineral deposits and zones of economic mineralization using geophysical remote sensing technology.

The idea that IP effect may be used to separate the responses of economic polarized targets from other anomalies was introduced in the pioneering papers by Zonge and Wynn, 1975, and Pelton et al., 1978. However, until recently this idea had very limited practical applications because of the difficulties in recovering the induced polarization parameters from the observed electromagnetic (EM) data, especially in the case of 3-D interpretation required for efficient exploration of the mining targets, and because of the absence of the adequate composite conductivity models of the rock formations.

The analysis of IP phenomena is usually based on models with frequency

dependent complex conductivity distribution. One of the most popular is the Cole-Cole relaxation model and its different modifications (Cole and Cole, 1941). The parameters of the conductivity relaxation model can be used for discrimination of the different types of rock formations, which is an important goal in mineral exploration. Until recently, these parameters have been determined mostly in the physical lab by direct analysis of the rock samples. In this project we develop and investigate a new geophysical technique for determining the 3-D distribution of the same parameters of rock formations in the field from geophysical observations.

We have developed a new composite geoelectrical model of rock formations based on the effective medium theory (EMT), which generates a conductivity relaxation model with the parameters directly related by analytical expressions to the physical characteristics of microstructure of the rocks and minerals (microgeometry and conductivity parameters). A new composite geoelectrical model provides more realistic representation of the complex rock formations than conventional unimodal conductivity models. It allows us to model the relationships between the physical characteristics of different types of rocks and minerals (e.g. conductivities, grain sizes, porosity, anisotropy, and polarizability) and the parameters of the relaxation model.

Effective-medium approximation for composite media has been discussed in many publications. The general formalism of the EMT was developed by Stroud (1975). The advances of physical effective-medium theories (e.g.. Norris et al., 1985; Shwartz, 1994; Kolundzija and Djordjevic, 2002) make it possible to develop a rigorous mathematical model of multi-phase heterogeneous conductive media excited by a transient EM field. The EMT was successfully applied to studying macroscopically isotropic and anisotropic models of rock formations in electrical geophysics (Mendelson and Cohen, 1982; Sen et al., 1981; Sheng, 1991; etc.). However, the existing form of EMT does not allow including the polarizability effect in the general model of heterogeneous rocks.

In this project we have developed a new generalized effective-medium theory of IP effect (GEMTIP) which takes into account the formation polarizability, as well. The general character of the proposed theory makes it possible to apply the developed results to study the rocks typical for mineralization zones and hydrocarbon reservoirs. This new generalized effective-medium theory of the IP effect (GEMTIP) allows us to develop a unified physical-mathematical model which can be used for examining the EM field propagation in complex rock formations with different mineral structures and electrical properties.

We demonstrate in the project that the goal of the EM geophysical survey is to determine the electrical conductivity and the intrinsic chargeability distributions as well as the other parameters of the relaxation model simultaneously. The recovered parameters of the relaxation model can be used for the discrimination of different rocks, and in this way will provide the ability to distinguish between uneconomic mineral deposits and zones of economic mineralization using geophysical remote sensing technology.

The solution of this problem requires development of effective numerical

methods for EM forward modeling and inversion in inhomogeneous media. During the first two years of the project, we have developed an appropriate numerical method for modeling the EM field in complex 3-D geoelectrical structures formed by inhomogeneous polarizable formations. Our method is based on the integral equation (IE) approach to numerical modeling, which provides the most accurate technique for EM field computer simulation.

In summary, during the first two research years of the project, our efforts were focused on developing the new generalized effective-medium theory of induced polarization (GEMTIP) and constructing an effective numerical method for fast and accurate modeling of the IP effect for different complex 3-D geoelectrical structures. This final technical report contains a description of the results of our study.

Professors Michael S. Zhdanov and Erich U. Petersen, as well as the following graduate students and postdoctoral fellows contributed to this research projects: Abraham Emond (M. S.), Seong Kon Lee (postdoc.), Takumi Ueda (Ph. D.), and Ken Yoshioka (postdoc.).

2. EXECUTIVE SUMMARY

In this report we summarize all work performed during the first two years of the project. Our research was focused on developing the foundations of a new geophysical technique for mineral exploration and mineral discrimination, based on electromagnetic methods. The developed new technique is based on examining the spectral induced polarization effects in electromagnetic data using modern distributed acquisition systems and advanced methods of 3-D inversion.

Mineral exploration needs a reliable method to distinguish between uneconomic mineral deposits and economic mineralization. Our technology consists of a new geophysical technique for subsurface material characterization, mineral exploration and discrimination which is based on a new composite geoelectrical model of rock formations generating a conductivity relaxation model with the parameters directly related by analytical expressions to the physical characteristics of the microstructure of the rocks and minerals (micro geometry and conductivity parameters). The new technique introduced in this project detects induced polarization effects in electromagnetic data and uses remote geophysical observations to determine the parameters of the conductivity relaxation model. These parameters are ultimately used for the discrimination of different rocks.

The solution of this problem requires development of effective numerical methods for EM forward modeling in 3-D inhomogeneous media. During the first two years of the project we have developed a prototype 3-D IP modeling algorithm using the integral equation (IE) method. Our IE forward modeling software is based on the contraction IE method, which improves the convergence rate of the iterative solvers. This software can handle various types of sources and receivers to compute the effect of a complex resistivity model. We have tested the working version of the software for computer simulation of the IP data for several models of typical mineral deposits.

We have developed a generalized effective medium theory of the induced polarization (IP) effect and electromagnetic (EM) field propagation in heterogenous polarizable media (GEMTIP). This new theory allows us to incorporate in the physical-mathematical model of the rock such rock-scale parameters as mineralization and/or fluid content, matrix composition, porosity, anisotropy, and the polarizability of the formations. Thus, GEMTIP in combination with the IE forward modeling method can be used for rock-scale forward modeling from grain-scale parameters.

As an illustration of the developed theory and methods, we have conducted deposit-scale modeling for a porphyry copper system in the southwestern U. S. This model is characterized by potentially strong EM coupling as well as IP effects. We have also simulated an EM-IP survey above a Kambalda-style,

nickel sulfide deposit located beneath a complicated regolith horizon. The numerical modeling study lays a background for future development of the EM-IP inversion method, directed at determining the electrical conductivity and the intrinsic chargeability distributions, as well as the other parameters of the relaxation model simultaneously.

The main conclusion of this research is that induced polarization effects in electromagnetic data can be effectively used for remote measuring the complex frequency dependent electrical conductivity of the rocks. An important result of this project includes a new generalized effective-medium theory of the IP effect (GEMTIP), which treats in a unified way different complex models of the multiphase composite models of the rocks. These new model and method can be used for examining the IP effect in complex rock formations with different mineral structures and electrical properties.

The new technology introduced in this project can be applied for interpretation of the ground, borehole, and airborne EM data. The recovered parameters of the relaxation model are used for the discrimination of different rocks, and in this way provide an ability to distinguish between uneconomic mineral deposits and zones of economic mineralization using geophysical remote sensing technology.

3. THEORY

The electromagnetic data observed in geophysical experiments, in general, reflect two phenomena: 1) electromagnetic induction (EMI) in the earth, and 2) induced polarization (IP) effect related to the relaxation of polarized charges in rock formations (Zonge and Wynn, 1975). The IP effect is caused by the complex physical-chemical polarization process that accompanies current flow in the earth. These reactions take place in a heterogeneous medium representing the rock formations in the areas of mineralization.

It is well known that the effective conductivity of rocks is not necessarily a constant and real number but may vary with frequency and be complex. There are several explanations for these properties of effective conductivity. Most often they are explained by the physical-chemical polarization effects of mineralized particles of the rock material, and/or by the electrokinetic effects in the poroses of reservoirs (Wait, 1959; Marshall and Madden, 1959; Luo and Zhang, 1998). This phenomenon is usually explained as a surface polarization of the mineralized particles, which occurs under the influence of the external electromagnetic field. It is manifested by accumulating electric charges on the surface of different grains forming the rock.

The development of the IP method can be traced back to the 1950s, when both mining and petroleum companies were actively looking into the application of this method to mineral exploration. The physical-mathematical principles of the IP effect were originally formulated in pioneering works by Wait (1959) and Sheinman (1969). However, this method did not find wide application in US industry until after the work of Zonge and his associates at the Zonge Engineering and Research Organization (Zonge and Wynn, 1975) and Pelton et al. (1978) at the University of Utah. Significant contribution to the development of the IP method was made, also, by Wait (1959, 1982), and by the research team at Kennecott in 1965-1977 (Nelson, 1997). The IP method has found wide application in mining exploration. A number of successful applications in hydrocarbon exploration were reported by Russian geophysicists (e.g. Komarov, 1980; Zonge, 1983; Kamenetsky, 1997; Davydycheva et al., 2004) as well.

The IP phenomenon is usually associated with charging and discharging effects in the ground in the process of current injecting. This phenomenon is usually explained as membrane polarization, which occurs when a pore space narrows to within several boundary layers of thickness, or as electrode polarization, which occurs when a pore space is blocked by metallic particles. We will demonstrate below, however, that the same phenomenon can be mathematically explained by the new generalized effective-medium theory of the IP effect developed as a result of this project.

3.1 Generalized effective-medium theory of the complex resistivity of multi-phase heterogeneous rocks

Effective-medium approximation for composite media has been discussed in many publications. The general formalism of the effective-medium theory (EMT) was introduced by Stroud (1975). The advances of physical effective-medium theories (e.g.. Norris et al., 1985; Shwartz, 1994; Kolundzija and Djordjevic, 2002) make it possible to develop a rigorous mathematical model of multi-phase heterogeneous conductive media excited by a transient EM field. The EMT was successfully applied to studying macroscopically isotropic and anisotropic models of rock formations in electrical geophysics (Mendelson and Cohen, 1982; Sen et al., 1981; Sheng, 1991; Kazatchenko et al., 2004; etc.). However, the existing form of EMT does not allow including the polarizability effect in the general model of heterogeneous rocks.

It is well known, however, that the effective conductivity of rocks is not necessarily a constant and real number but may vary with frequency and be complex (Shuev and Johnson, 1973). There are several explanations for these properties of effective conductivity. Most often they are explained by the physical-chemical polarization effects of mineralized particles of the rock material, and/or by the electrokinetic effects in the poroses of reservoirs (Wait, 1959; Marshall and Madden, 1959; Luo and Zhang, 1998). Thus, the polarizability is caused by the complex electrochemical reactions that accompany current flow in the earth. These reactions take place in a heterogeneous medium representing the rock formations in the areas of mineralization. Under the influence of the external electromagnetic field, a surface polarization of the mineralized particles and the surface of the moisture-porous space occurs. It is manifested by accumulating electric charges on the surface of different grains forming the rock. This effect is very significant in the case of metal-electrolyte interface (Bockrih and Reddy, 1973). However, a similar effect is observed in the case of the interface between electrolyte and typical rock-forming minerals like silicate, carbonate, and others (Komarov, 1980).

It is demonstrated in this report that EMT formalism can be used in the theory of formation polarizability, as well. The general character of the proposed model makes it possible to apply the developed results to study the rocks typical for mineralization zones and hydrocarbon reservoirs. This new theory allows us to develop a unified physical-mathematical model which can be used for examining the EM effects in complex rock formations with different mineral structures and electrical properties. It takes into account the mineralization and/or fluid content of the rocks, the matrix composition, porosity, anisotropy, and polarizability of the formations. This approach allows us to provide a link between the volume content of different minerals and/or the hydrocarbon

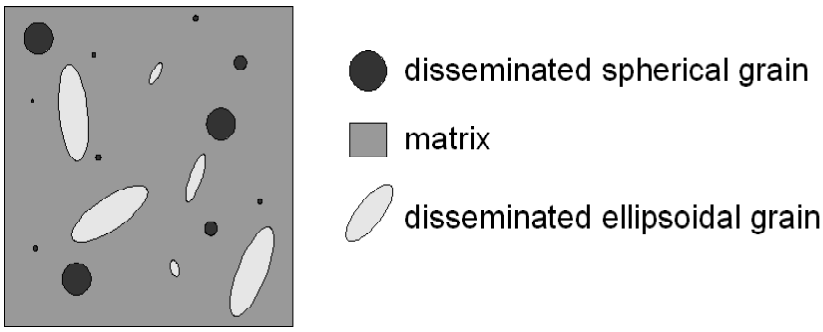

Figure 3-1 A typical example of a multi-phase model of the rock composed of a set of different types of randomly oriented grains.

saturation and the observed EM field data (Zhdanov, 2005).

3.1.1 Principles of the effective-medium approach

We represent a complex heterogeneous rock formation as a composite model formed by a homogeneous host medium of a volume V with a (complex) conductivity tensor $\widehat{\boldsymbol{\sigma}}_0(\mathbf{r})$ (where $\mathbf{r}$ is an observation point) filled with grains of arbitrary shape and conductivity. A typical example of a multi-phase model of the rock is shown in Figure 3-1.

In the present problem, the rock is composed of a set of N different types of grains, the lth grain type having (complex) tensor conductivity $\widehat{\boldsymbol{\sigma}}_l$. The grains of the lth type have a volume fraction f_l in the medium and a particular shape and orientation. Therefore, the total conductivity tensor of the model, $\widehat{\boldsymbol{\sigma}}(\mathbf{r})$, has the following distribution for volume fraction f_l and volume fraction $f_0 = \left(1 - \sum_{l=1}^{N} f_l\right)$, respectively:

$$\widehat{\boldsymbol{\sigma}}(\mathbf{r}) = \begin{cases} \widehat{\boldsymbol{\sigma}}_0 \text{ for volume fraction } f_0 = \left(1 - \sum_{l=1}^{N} f_l\right) \\ \\ \widehat{\boldsymbol{\sigma}}_l \text{ for volume fraction } f_l\,. \end{cases} \tag{3.1}$$

The polarizability effect is usually associated with surface polarization of the coatings of the grains. This surface polarization can be related to electrochemical charge transfer between the grains and a host medium. (Wong, 1979; Wong and Strangway, 1981; Klein et al., 1984). The surface polarization is manifested by accumulating electric charges on the surface of the grain. A double layer of charges is created on the grain's surface, which results in the voltage drop at this surface (Wait, 1982). It has been shown experimentally that for relatively small external electric fields used in electrical exploration, the voltage drop, Δu, is linear proportional to the normal current flow at the

surface of the particle, $j_n = (\mathbf{n} \cdot \mathbf{j})$. That is, at the surface of the grain we have

$$\Delta u = k \left(\mathbf{n} \cdot \mathbf{j} \right), \tag{3.2}$$

where $\mathbf{n}$ is a unit vector of the outer normal to the grain's surface, and k is a surface polarizability factor, which, in general, is a complex frequency dependent function. This function is usually treated as the interface impedance which characterizes the boundary between the corresponding grain and surrounding host medium and describes the interfacial or membrane polarization. This effect is the most profound in the case of metal-electrolyte interface, and it was intensively studied in electrochemistry (Bockrih and Reddy, 1973; Madden and Marshall, 1959). However, a similar effect was found in other heterogeneous systems typical for rock formations, as well (e.g., Dukhin, 1971).

Following the standard logic of the EMT, we substitute a homogeneous effective medium with the conductivity tensor $\widehat{\boldsymbol{\sigma}}_e$ for the original heterogeneous composite model and subject it to a constant electric field, $\mathbf{E}^b$, equal to the average electric field in the original model:

$$\mathbf{E}^b = \langle \mathbf{E} \rangle = V^{-1} \iiint_V \mathbf{E} \left(\mathbf{r} \right) dv. \tag{3.3}$$

The effective conductivity is defined from the condition that the current density distribution $\mathbf{j}_e$ in an effective medium is equal to the average current density distribution in the original model:

$$\mathbf{j}_e = \widehat{\boldsymbol{\sigma}}_e \cdot \mathbf{E}^b = \widehat{\boldsymbol{\sigma}}_e \cdot \langle \mathbf{E} \rangle = \langle \widehat{\boldsymbol{\sigma}} \cdot \mathbf{E} \rangle . \tag{3.4}$$

In order to find the effective conductivity tensor $\widehat{\boldsymbol{\sigma}}_e$, we represent the given inhomogeneous composite model as a superposition of a homogeneous infinite background medium with the conductivity tensor $\widehat{\boldsymbol{\sigma}}_b$ and the anomalous conductivity $\Delta \widehat{\boldsymbol{\sigma}} \left(\mathbf{r} \right)$:

$$\widehat{\boldsymbol{\sigma}} \left(\mathbf{r} \right) = \widehat{\boldsymbol{\sigma}}_b + \Delta \widehat{\boldsymbol{\sigma}} \left(\mathbf{r} \right). \tag{3.5}$$

Note that this representation is not unique. There exist different methods of selecting the appropriate background conductivity $\widehat{\boldsymbol{\sigma}}_b$, which we will discuss below.

From (3.5) and (3.4), we have:

$$\widehat{\boldsymbol{\sigma}}_e \cdot \mathbf{E}^b = \widehat{\boldsymbol{\sigma}}_b \cdot \mathbf{E}^b + \langle \Delta \widehat{\boldsymbol{\sigma}} \cdot \mathbf{E} \rangle . \tag{3.6}$$

Thus, we can see that the effective conductivity tensor, $\widehat{\boldsymbol{\sigma}}_e$, can be found from equation (3.6), if one determines the average excess electric current $\langle \Delta \widehat{\boldsymbol{\sigma}} \cdot \mathbf{E} \rangle$. The last problem can be solved using the integral form of Maxwell's equations.

Following the ideas of the QL approximation (Zhdanov, 2002), we can represent the electric field as:

$$\mathbf{E} \left(\mathbf{r}' \right) = \left(\widehat{\mathbf{I}} + \widehat{\boldsymbol{\lambda}} \left(\mathbf{r}' \right) \right) \cdot \mathbf{E}^b, \tag{3.7}$$

where $\widehat{\boldsymbol{\lambda}}(\mathbf{r}')$ is the electrical reflectivity coefficient, and:

$$\Delta\widehat{\boldsymbol{\sigma}}(\mathbf{r}')\cdot\mathbf{E}(\mathbf{r}')=\widehat{\mathbf{m}}(\mathbf{r}')\cdot\mathbf{E}^b, \tag{3.8}$$

where $\widehat{\mathbf{m}}(\mathbf{r}')$ is the material property tensor (which is similar to the susceptibility tensor in the theory of the EM field propagation in dielectrics):

$$\widehat{\mathbf{m}}(\mathbf{r}')=\Delta\widehat{\boldsymbol{\sigma}}(\mathbf{r}')\cdot\left(\widehat{\mathbf{I}}+\widehat{\boldsymbol{\lambda}}(\mathbf{r}')\right). \tag{3.9}$$

Note that the exact representation (3.8) always exists because the corresponding material property tensor can always be found for any given fields $\mathbf{E}(\mathbf{r}')$ and $\mathbf{E}^b$ (Zhdanov, 2002).

Let us substitute (3.8) into (3.4), taking into account (3.5):

$$\mathbf{j}_e=\widehat{\boldsymbol{\sigma}}_e\cdot\mathbf{E}^b=\langle\widehat{\boldsymbol{\sigma}}\cdot\mathbf{E}\rangle=\langle(\widehat{\boldsymbol{\sigma}}_b+\Delta\widehat{\boldsymbol{\sigma}})\cdot\mathbf{E}\rangle=$$

$$\widehat{\boldsymbol{\sigma}}_b\cdot\langle\mathbf{E}\rangle+\langle\Delta\widehat{\boldsymbol{\sigma}}\cdot\mathbf{E}\rangle=\widehat{\boldsymbol{\sigma}}_b\cdot\mathbf{E}^b+\langle\widehat{\mathbf{m}}\rangle\cdot\mathbf{E}^b.$$

From the last formula we see that:

$$\widehat{\boldsymbol{\sigma}}_e=\widehat{\boldsymbol{\sigma}}_b+\langle\widehat{\mathbf{m}}\rangle. \tag{3.10}$$

Thus, in order to determine the effective conductivity of the composite polarized medium, we have to find the average value of the material property tensor, $\langle\widehat{\mathbf{m}}\rangle$.

3.1.2 Integral representations for the EM field in heterogenous polarizable media

One can represent the electric field $\mathbf{E}(\mathbf{r})$ generated in a homogeneous anisotropic background medium by the currents induced within the anomalous conductivity $\Delta\widehat{\boldsymbol{\sigma}}(\mathbf{r})$ using an integral form of the Maxwell's equations:

$$\mathbf{E}(\mathbf{r})=\mathbf{E}^b+\iiint_V\widehat{\mathbf{G}}_b(\mathbf{r}\mid\mathbf{r}')\cdot[\Delta\widehat{\boldsymbol{\sigma}}(\mathbf{r}')\cdot\mathbf{E}(\mathbf{r}')]\,dv', \tag{3.11}$$

where V is the volume occupied by all inhomogeneities, and $\widehat{\mathbf{G}}_b(\mathbf{r}\mid\mathbf{r}')$ is a Green's tensor for the homogeneous anisotropic full space.

In order to simplify the further discussion, we assume that the background model is represented by the isotropic homogeneous full space: $\widehat{\boldsymbol{\sigma}}_b=\widehat{\mathbf{I}}\sigma_b$. In this case the Green's tensor can be represented in the form of a dyadic function:

$$\widehat{\mathbf{G}}_b(\mathbf{r}\mid\mathbf{r}')=\nabla\nabla' g_b(\mathbf{r}\mid\mathbf{r}'), \tag{3.12}$$

where:

$$g_b(\mathbf{r}\mid\mathbf{r}')=\frac{1}{4\pi\sigma_b|\mathbf{r}-\mathbf{r}'|}. \tag{3.13}$$

We assume, however, that in addition to electrical heterogeneity, the medium is characterized by polarizability effects which are manifested by the surface polarization of the grains. Mathematically, the surface polarization effect can be included in the general system of Maxwell's equations by adding the following boundary conditions on the surfaces S_l of the grains (Luo and Zhang, 1998):

$$\left[\mathbf{n}\times\left(\mathbf{E}^{+}\left(\mathbf{r}'\right)-\mathbf{E}^{-}\left(\mathbf{r}'\right)\right)\right]_{S_l}=-\left[\mathbf{n}\times\boldsymbol{\nabla}'\Delta u\left(\mathbf{r}'\right)\right]_{S_l}, \tag{3.14}$$

where $\mathbf{E}^{+}$ designates the boundary value of electric field $\mathbf{E}\left(\mathbf{r}\right)$ when the observation point tends to the boundary S_l of the lth grain from the inside of the grains, and $\mathbf{E}^{-}$ if this point tends to the boundary from the outside of the grains.

Therefore, the electric field due to the surface polarization effect $\mathbf{E}^{p}\left(\mathbf{r}\right)$ can be represented as an electric field of a specified discontinuity (3.14) (Zhdanov, 1988, p. 250):

$$\mathbf{E}^{p}\left(\mathbf{r}\right)=-\boldsymbol{\nabla}\times\iint_{S}g_b\left(\mathbf{r}\mid\mathbf{r}'\right)\sigma_b\left[\mathbf{n}\left(\mathbf{r}'\right)\cdot\left(\mathbf{E}^{+}\left(\mathbf{r}'\right)-\mathbf{E}^{-}\left(\mathbf{r}'\right)\right)\right]_{S}ds', \tag{3.15}$$

where S stands for the superposition of all surfaces S_l of the entire ensemble of grains, $S=\overset{N}{\underset{l=1}{\cup}}S_l$, and vector $\mathbf{n}\left(\mathbf{r}'\right)$ is directed outside the grains.

The last integral can be written in an equivalent form as a field generated by the double layers coinciding with the grains' surfaces with a dipole electric charge moment density $\mathbf{M}_S=\Delta u\mathbf{n}$ (Zhdanov, 1988, p. 144):

$$\mathbf{E}^{p}\left(\mathbf{r}\right)=\boldsymbol{\nabla}\iint_{S}\boldsymbol{\nabla}'g_b\left(\mathbf{r}\mid\mathbf{r}'\right)\sigma_b\cdot\mathbf{n}\left(\mathbf{r}'\right)\Delta uds'. \tag{3.16}$$

According to (3.2), we assume that the voltage drop at the surface of the grain is proportional to the normal current:

$$\Delta u=k\left(\mathbf{n}\left(\mathbf{r}'\right)\cdot\mathbf{j}\left(\mathbf{r}'\right)\right)=k\left(\mathbf{n}\left(\mathbf{r}'\right)\cdot\widehat{\boldsymbol{\sigma}}\left(\mathbf{r}'\right)\cdot\mathbf{E}\left(\mathbf{r}'\right)\right), \tag{3.17}$$

where current $\mathbf{j}\left(\mathbf{r}'\right)$ is taken for the internal side of the grain's surface.

Therefore, expression (3.15) becomes:

$$\mathbf{E}^{p}\left(\mathbf{r}\right)=\boldsymbol{\nabla}\iint_{S}\boldsymbol{\nabla}'g_b\left(\mathbf{r}\mid\mathbf{r}'\right)\sigma_b\cdot\mathbf{n}\left(\mathbf{r}'\right)\Delta uds'=$$

$$\iint_{S}\widehat{\mathbf{G}}_b\left(\mathbf{r}\mid\mathbf{r}'\right)\cdot\mathbf{n}\left(\mathbf{r}'\right)k\sigma_b\left(\mathbf{n}\left(\mathbf{r}'\right)\cdot\widehat{\boldsymbol{\sigma}}\left(\mathbf{r}'\right)\cdot\mathbf{E}\left(\mathbf{r}'\right)\right)ds'. \tag{3.18}$$

The total electric field caused by the effects of both the electromagnetic induction and induced polarization is equal to:

$$\mathbf{E}\left(\mathbf{r}\right)=\mathbf{E}^{b}+\iiint_{V}\widehat{\mathbf{G}}_b\left(\mathbf{r}\mid\mathbf{r}'\right)\cdot\left[\Delta\widehat{\boldsymbol{\sigma}}\left(\mathbf{r}'\right)\cdot\mathbf{E}\left(\mathbf{r}'\right)\right]dv'+$$

$$\iint_{S}\widehat{\mathbf{G}}_b\left(\mathbf{r}\mid\mathbf{r}'\right)\cdot\mathbf{n}\left(\mathbf{r}'\right)k\sigma_b\left(\mathbf{n}\left(\mathbf{r}'\right)\cdot\widehat{\boldsymbol{\sigma}}\left(\mathbf{r}'\right)\cdot\mathbf{E}\left(\mathbf{r}'\right)\right)ds'. \tag{3.19}$$

Substituting expression (3.8) into formula (3.19), we can write:

$$\mathbf{E}(\mathbf{r}) = \mathbf{E}^b + \iiint_V \widehat{\mathbf{G}}_b(\mathbf{r} \mid \mathbf{r}') \cdot \left[\widehat{\mathbf{m}}(\mathbf{r}') \cdot \mathbf{E}^b\right] dv' +$$

$$\iint_S \widehat{\mathbf{G}}_b(\mathbf{r} \mid \mathbf{r}') \cdot \mathbf{n}(\mathbf{r}') \left(\mathbf{n}(\mathbf{r}') \cdot \widehat{\boldsymbol{\xi}}(\mathbf{r}') \cdot \left[\widehat{\mathbf{m}}(\mathbf{r}') \cdot \mathbf{E}^b\right]\right) ds', \tag{3.20}$$

where $\widehat{\boldsymbol{\xi}}(\mathbf{r}')$ is equal to:

$$\widehat{\boldsymbol{\xi}}(\mathbf{r}') = k\sigma_b \widehat{\boldsymbol{\sigma}}(\mathbf{r}') \cdot (\Delta\widehat{\boldsymbol{\sigma}}(\mathbf{r}'))^{-1}. \tag{3.21}$$

We can represent the integrals in equation (3.20) as a sum of the integrals over the volumes and surfaces of all grains:

$$\mathbf{E}(\mathbf{r}) = \mathbf{E}^b + \sum_l \mathbf{E}_l(\mathbf{r}), \tag{3.22}$$

where:

$$\mathbf{E}_l(\mathbf{r}) = \iiint_{V_l} \widehat{\mathbf{G}}_b(\mathbf{r} \mid \mathbf{r}') \cdot \left[\widehat{\mathbf{m}}(\mathbf{r}') \cdot \mathbf{E}^b\right] dv' +$$

$$\iint_{S_l} \widehat{\mathbf{G}}_b(\mathbf{r} \mid \mathbf{r}') \cdot \mathbf{n}(\mathbf{r}') \left(\mathbf{n}(\mathbf{r}') \cdot \widehat{\boldsymbol{\xi}}(\mathbf{r}') \cdot \left[\widehat{\mathbf{m}}(\mathbf{r}') \cdot \mathbf{E}^b\right]\right) ds'. \tag{3.23}$$

As usual, we restrict our discussion to the low frequency approximation (quasi-static model of the field), where $a_l/w_l << 1$; a_l is a characteristic size of a grain of the lth type, and w_l is a wavelength in that grain. In this case, we can use a QL approximation for the integrals over V_l and S_l and assume that the material property tensor is constant in V_l up to its boundary S_l :

$$\widehat{\mathbf{m}}(\mathbf{r}') = \widehat{\mathbf{m}}_l, \ , \ \mathbf{r}' \in V_l. \tag{3.24}$$

Note, however, that in the case of spherical or elliptical grains the material property tensor is always constant within the spherical and/or elliptical inclusions.

Consider now the integrals over one grain only:

$$\mathbf{E}_l(\mathbf{r}) = \iiint_{V_l} \widehat{\mathbf{G}}_b(\mathbf{r} \mid \mathbf{r}')\, dv' \cdot \widehat{\mathbf{m}}_l \cdot \mathbf{E}^b +$$

$$\iint_{S_l} \widehat{\mathbf{G}}_b(\mathbf{r} \mid \mathbf{r}') \cdot \mathbf{n}(\mathbf{r'})\, \mathbf{n}(\mathbf{r}')\, ds' \cdot \widehat{\boldsymbol{\xi}}_l \cdot \widehat{\mathbf{m}}_l \cdot \mathbf{E}^b, \tag{3.25}$$

where:

$$\widehat{\boldsymbol{\xi}}(\mathbf{r}') = \widehat{\boldsymbol{\xi}}_l = const, \ \ \mathbf{r}' \in V_l.$$

We introduce the volume, $\widehat{\boldsymbol{\Gamma}}_l$, and surface, $\widehat{\boldsymbol{\Lambda}}_l$, depolarization tensors as follows:

$$\widehat{\boldsymbol{\Gamma}}_l = \iiint_{V_l} \widehat{\mathbf{G}}_b(\mathbf{r} \mid \mathbf{r}')\, dv', \tag{3.26}$$

and:

$$\widehat{\boldsymbol{\Lambda}}_l = \iint_{S_l} \widehat{\mathbf{G}}_b(\mathbf{r} \mid \mathbf{r}') \cdot \mathbf{n}(\mathbf{r}')\, \mathbf{n}(\mathbf{r}')\, ds'. \tag{3.27}$$

For example, for a spherical grain of a radius a_l, we have (see Appendix):

$$\widehat{\mathbf{\Gamma}}_l = -\frac{1}{3\sigma_b}\widehat{\mathbf{I}},\ \widehat{\mathbf{\Lambda}}_l = -\frac{2}{3\sigma_b a_l}\widehat{\mathbf{I}}. \tag{3.28}$$

Substituting (3.26) and (3.27) back into (3.25), we obtain:

$$\mathbf{E}_l(\mathbf{r}) = \widehat{\mathbf{\Gamma}}_l \cdot \widehat{\mathbf{m}}_l \cdot \mathbf{E}^b + \widehat{\mathbf{\Gamma}}_l \cdot \widehat{\mathbf{p}}_l \cdot \widehat{\mathbf{m}}_l \cdot \mathbf{E}^b = \widehat{\mathbf{\Gamma}}_l \cdot \widehat{\mathbf{q}}_l \cdot \mathbf{E}^b, \tag{3.29}$$

where a surface polarizability tensor $\widehat{\mathbf{p}}$ and a volume polarizability tensor $\widehat{\mathbf{q}}$ are equal to:

$$\widehat{\mathbf{p}}(\mathbf{r}') = \widehat{\mathbf{\Gamma}}_l^{-1} \cdot \widehat{\mathbf{\Lambda}}_l \cdot \widehat{\boldsymbol{\xi}}(\mathbf{r}'),\ \widehat{\mathbf{p}}_l = \widehat{\mathbf{p}}(\mathbf{r}'),\ \mathbf{r}' \in V_l, \tag{3.30}$$

and

$$\widehat{\mathbf{q}}(\mathbf{r}') = \left[\widehat{\mathbf{I}} + \widehat{\mathbf{p}}(\mathbf{r}')\right] \cdot \widehat{\mathbf{m}}(\mathbf{r}'),\ \widehat{\mathbf{q}}_l = \widehat{\mathbf{q}}(\mathbf{r}'),\ \mathbf{r}' \in V_l. \tag{3.31}$$

Then formula (3.29) becomes:

$$\mathbf{E}_l(\mathbf{r}) = \iiint_{V_l} \widehat{\mathbf{G}}_b(\mathbf{r} \mid \mathbf{r}')\, dv' \cdot \widehat{\mathbf{q}}_l \cdot \mathbf{E}^b. \tag{3.32}$$

Substituting expression (3.32) back into (3.22), we find:

$$\mathbf{E}(\mathbf{r}) = \mathbf{E}^b + \sum_l \iiint_{V_l} \widehat{\mathbf{G}}_b(\mathbf{r} \mid \mathbf{r}') \cdot \widehat{\mathbf{q}}(\mathbf{r}')\, dv' \cdot \mathbf{E}^b =$$

$$\mathbf{E}^b + \iiint_V \widehat{\mathbf{G}}_b(\mathbf{r} \mid \mathbf{r}') \cdot \widehat{\mathbf{q}}(\mathbf{r}')\, dv' \cdot \mathbf{E}^b. \tag{3.33}$$

The last formula shows that the surface polarization effect introduced by formula (3.18) can be represented by the equivalent volume polarization effect and combined with the electromagnetic induction phenomenon in one integral expression.

3.1.3 Effective conductivity of the heterogeneous polarizable medium

In this section we will derive a constructive approach for determining the effective conductivity of the heterogeneous polarizable medium. We have established above that, in order to solve this problem, we have to find the average value of the material property tensor, $\langle\widehat{\mathbf{m}}\rangle$. The last function can be found based on the integral representation (3.33).

Multiplying both sides of (3.33) by $\Delta\widehat{\boldsymbol{\sigma}}(\mathbf{r})$, we have:

$$\widehat{\mathbf{m}}(\mathbf{r}) \cdot \mathbf{E}^b = \Delta\widehat{\boldsymbol{\sigma}}(\mathbf{r}) \cdot \mathbf{E}^b + \Delta\widehat{\boldsymbol{\sigma}}(\mathbf{r}) \cdot \iiint_V \widehat{\mathbf{G}}_b(\mathbf{r} \mid \mathbf{r}') \cdot \widehat{\mathbf{q}}(\mathbf{r}')\, dv' \cdot \mathbf{E}^b. \tag{3.34}$$

Our goal is to find the material property tensor $\widehat{\mathbf{m}}$. According to equation (3.31), this tensor is related to the volume polarizability tensor $\widehat{\mathbf{q}}$ by the following formula:

$$\widehat{\mathbf{m}} = \left[\widehat{\mathbf{I}} + \widehat{\mathbf{p}}\right]^{-1} \widehat{\mathbf{q}}. \tag{3.35}$$

Therefore, in order to find $\widehat{\mathbf{m}}$, we need to determine tensor $\widehat{\mathbf{q}}$ first. Multiplying both sides of (3.34) by $\left[\widehat{\mathbf{I}}+\widehat{\mathbf{p}}\right]$, we finally arrive at the equation for $\widehat{\mathbf{q}}$:

$$\widehat{\mathbf{q}}\left(\mathbf{r}\right)=\Delta\widehat{\boldsymbol{\sigma}}^{p}\left(\mathbf{r}\right)+\Delta\widehat{\boldsymbol{\sigma}}^{p}\left(\mathbf{r}\right)\cdot\iiint_{V}\widehat{\mathbf{G}}_{b}\left(\mathbf{r}\mid\mathbf{r}'\right)\cdot\widehat{\mathbf{q}}\left(\mathbf{r}'\right)dv', \tag{3.36}$$

where $\Delta\widehat{\boldsymbol{\sigma}}^{p}\left(\mathbf{r}\right)$ is a "polarized" anomalous conductivity:

$$\Delta\widehat{\boldsymbol{\sigma}}^{p}\left(\mathbf{r}\right)=\left[\widehat{\mathbf{I}}+\widehat{\mathbf{p}}\left(\mathbf{r}\right)\right]\cdot\Delta\widehat{\boldsymbol{\sigma}}\left(\mathbf{r}\right). \tag{3.37}$$

The volume integral in equation (3.36) can be represented as a sum of two integrals: over the volume of one grain, V_l, and over the remaining volume $(V-V_l)$:

$$\iiint_{V}\widehat{\mathbf{G}}_{b}\left(\mathbf{r}\mid\mathbf{r}'\right)\cdot\widehat{\mathbf{q}}\left(\mathbf{r}'\right)dv'=$$

$$\iiint_{V-V_l}\widehat{\mathbf{G}}_{b}\left(\mathbf{r}\mid\mathbf{r}'\right)\cdot\widehat{\mathbf{q}}\left(\mathbf{r}'\right)dv'+\iiint_{V_l}\widehat{\mathbf{G}}_{b}\left(\mathbf{r}\mid\mathbf{r}'\right)\cdot\widehat{\mathbf{q}}\left(\mathbf{r}'\right)dv'. \tag{3.38}$$

We approximate the integral over $(V-V_l)$ by replacing $\widehat{\mathbf{q}}\left(\mathbf{r}'\right)$ by its average in V, and we calculate the integral over V_l, taking into account property (3.24): $\widehat{\mathbf{q}}\left(\mathbf{r}'\right)=\widehat{\mathbf{q}}_{l}=const$. As a result, we obtain:

$$\iiint_{V}\widehat{\mathbf{G}}_{b}\left(\mathbf{r}\mid\mathbf{r}'\right)\cdot\widehat{\mathbf{q}}\left(\mathbf{r}'\right)dv'\approx$$

$$\iiint_{V-V_l}\widehat{\mathbf{G}}_{b}\left(\mathbf{r}\mid\mathbf{r}'\right)dv'\cdot\langle\widehat{\mathbf{q}}\rangle+\iiint_{V_l}\widehat{\mathbf{G}}_{b}\left(\mathbf{r}\mid\mathbf{r}'\right)dv'\cdot\widehat{\mathbf{q}}_{l}. \tag{3.39}$$

According to the Gauss theorem, the volume depolarization tensor $\widehat{\mathbf{\Gamma}}_{l}$ is equal to:

$$\widehat{\mathbf{\Gamma}}_{l}=\nabla\iiint_{V_l}\nabla' g_{b}\left(\mathbf{r}\mid\mathbf{r}'\right)dv'=\nabla\iint_{S_l}g_{b}\left(\mathbf{r}\mid\mathbf{r}'\right)\mathbf{n}\left(\mathbf{r}'\right)ds'. \tag{3.40}$$

We can calculate the external integral in the limit of the infinitely large volume V in a similar way, using the Gauss theorem for the external domain $(V-V_l)$:

$$\iiint_{V-V_l}\widehat{\mathbf{G}}_{b}\left(\mathbf{r}\mid\mathbf{r}'\right)dv'=-\widehat{\mathbf{\Gamma}}_{l}. \tag{3.41}$$

Substituting equations (3.40) and (3.41) into (3.39), we have:

$$\iiint_{V}\widehat{\mathbf{G}}_{b}\left(\mathbf{r}\mid\mathbf{r}'\right)\cdot\widehat{\mathbf{q}}\left(\mathbf{r}'\right)dv'\approx-\widehat{\mathbf{\Gamma}}_{l}\cdot\langle\widehat{\mathbf{q}}\rangle+\widehat{\mathbf{\Gamma}}_{l}\cdot\widehat{\mathbf{q}}_{l}. \tag{3.42}$$

The last result reduces equation (3.36) to:

$$\widehat{\mathbf{q}}\left(\mathbf{r}\right)=\Delta\widehat{\boldsymbol{\sigma}}^{p}\left(\mathbf{r}\right)+\Delta\widehat{\boldsymbol{\sigma}}^{p}\left(\mathbf{r}\right)\cdot\widehat{\mathbf{\Gamma}}_{l}\cdot\left[\widehat{\mathbf{q}}_{l}-\langle\widehat{\mathbf{q}}\rangle\right]. \tag{3.43}$$

Assuming in the last formula that $\mathbf{r}\in V_l$, we find:

$$\widehat{\mathbf{q}}_{l}=\Delta\widehat{\boldsymbol{\sigma}}_{l}^{p}+\Delta\widehat{\boldsymbol{\sigma}}_{l}^{p}\cdot\widehat{\mathbf{\Gamma}}_{l}\cdot\left[\widehat{\mathbf{q}}_{l}-\langle\widehat{\mathbf{q}}\rangle\right]. \tag{3.44}$$

Solving equation (3.36), we determine the volume polarizability tensor, $\widehat{\mathbf{q}}_l$, for every grain:

$$\widehat{\mathbf{q}}_l = \left[\widehat{\mathbf{I}} - \Delta\widehat{\boldsymbol{\sigma}}_l^p \cdot \widehat{\boldsymbol{\Gamma}}_l\right]^{-1} \cdot \Delta\widehat{\boldsymbol{\sigma}}_l^p \cdot \left[\widehat{\mathbf{I}} - \widehat{\boldsymbol{\Gamma}}_l \cdot \langle\widehat{\mathbf{q}}\rangle\right]. \tag{3.45}$$

Taking an average value of both sides of (3.45), and solving the resulting equation for $\langle\widehat{\mathbf{q}}\rangle$, we finally find:

$$\langle\widehat{\mathbf{q}}\rangle = \left\langle\left[\widehat{\mathbf{I}} - \Delta\widehat{\boldsymbol{\sigma}}^p \cdot \widehat{\boldsymbol{\Gamma}}\right]^{-1}\right\rangle^{-1} \left\langle\left[\widehat{\mathbf{I}} - \Delta\widehat{\boldsymbol{\sigma}}^p \cdot \widehat{\boldsymbol{\Gamma}}\right]^{-1} \cdot \Delta\widehat{\boldsymbol{\sigma}}^p\right\rangle. \tag{3.46}$$

According to equation (3.31), the average value of the material property tensor is:

$$\langle\widehat{\mathbf{m}}\rangle = \left\langle\left[\widehat{\mathbf{I}} + \widehat{\mathbf{p}}\right]^{-1} \widehat{\mathbf{q}}\right\rangle. \tag{3.47}$$

Substituting (3.47) into (3.10), we finally have:

$$\widehat{\boldsymbol{\sigma}}_e = \widehat{\boldsymbol{\sigma}}_b + \left\langle\left[\widehat{\mathbf{I}} + \widehat{\mathbf{p}}\right]^{-1} \widehat{\mathbf{q}}\right\rangle =$$

$$\widehat{\boldsymbol{\sigma}}_b + \left[\widehat{\mathbf{I}} + \widehat{\mathbf{p}}_0\right]^{-1} \widehat{\mathbf{q}}_0 f_0 + \sum_{l=1}^{N} \left[\widehat{\mathbf{I}} + \widehat{\mathbf{p}}_l\right]^{-1} \widehat{\mathbf{q}}_l f_l. \tag{3.48}$$

Formula (3.10) allows us to calculate the effective conductivity for any multi-phase polarized composite medium. This formula can be treated as an IP analog of the "average-t-matrix approximation" (ATA) of the theory of electronic propagation in disordered binary alloys (Soven, 1967).

3.1.4 Self-consistent approximation for effective conductivity

Note that the simplest choice for the average value of the volume polarizability tensor $\langle\widehat{\mathbf{q}}\rangle$ is:

$$\langle\widehat{\mathbf{q}}\rangle = 0, \tag{3.49}$$

because in this case from (3.45) we have:

$$\widehat{\mathbf{q}}_l = \left[\widehat{\mathbf{I}} - \Delta\widehat{\boldsymbol{\sigma}}_l^p \cdot \widehat{\boldsymbol{\Gamma}}_l\right]^{-1} \cdot \Delta\widehat{\boldsymbol{\sigma}}_l^p, \tag{3.50}$$

and

$$\langle\widehat{\mathbf{q}}\rangle = \left\langle\left[\widehat{\mathbf{I}} - \Delta\widehat{\boldsymbol{\sigma}}^p \cdot \widehat{\boldsymbol{\Gamma}}\right]^{-1} \cdot \Delta\widehat{\boldsymbol{\sigma}}^p\right\rangle =$$

$$\left[\widehat{\mathbf{I}} - \Delta\widehat{\boldsymbol{\sigma}}_0^p \cdot \widehat{\boldsymbol{\Gamma}}_0\right]^{-1} f_0 + \sum_{l=1}^{N} \left[\widehat{\mathbf{I}} - \Delta\widehat{\boldsymbol{\sigma}}_l^p \cdot \widehat{\boldsymbol{\Gamma}}_l\right]^{-1} f_l = 0. \tag{3.51}$$

Equation (3.51) can be treated as a loose IP analog of the self-consistency condition of the conventional effective medium theory (Stroud, 1975). Detailed

analysis shows that for a composite medium without IP effect, equation (3.51) leads to the Bruggeman method of the effective conductivity determination (Choi, 1999).

Substituting (3.50) into (3.35), we find:

$$\widehat{\mathbf{m}}_l = \left[\widehat{\mathbf{I}} + \widehat{\mathbf{p}}_l\right]^{-1} \left[\widehat{\mathbf{I}} - \Delta\widehat{\boldsymbol{\sigma}}_l^p \cdot \widehat{\boldsymbol{\Gamma}}_l\right]^{-1} \cdot \left[\widehat{\mathbf{I}} + \widehat{\mathbf{p}}_l\right] \cdot \Delta\widehat{\boldsymbol{\sigma}}_l. \tag{3.52}$$

In this case, expression (3.10) for the effective conductivity of the polarized inhomogeneous medium takes the form:

$$\widehat{\boldsymbol{\sigma}}_e = \widehat{\boldsymbol{\sigma}}_b + \left[\widehat{\mathbf{I}} + \widehat{\mathbf{p}}_0\right]^{-1} \left[\widehat{\mathbf{I}} - \Delta\widehat{\boldsymbol{\sigma}}_0^p \cdot \widehat{\boldsymbol{\Gamma}}_0\right]^{-1} \cdot \left[\widehat{\mathbf{I}} + \widehat{\mathbf{p}}_0\right] \cdot \Delta\widehat{\boldsymbol{\sigma}}_0 f_0 +$$

$$\sum_{l=1}^{N} \left[\widehat{\mathbf{I}} + \widehat{\mathbf{p}}_l\right]^{-1} \left[\widehat{\mathbf{I}} - \Delta\widehat{\boldsymbol{\sigma}}_l^p \cdot \widehat{\boldsymbol{\Gamma}}_l\right]^{-1} \cdot \left[\widehat{\mathbf{I}} + \widehat{\mathbf{p}}_l\right] \cdot \Delta\widehat{\boldsymbol{\sigma}}_l f_l.$$

In particular, if we select the background conductivity to be equal to the host medium conductivity,

$$\widehat{\boldsymbol{\sigma}}_b = \widehat{\boldsymbol{\sigma}}_0,$$

then:

$$\widehat{\boldsymbol{\sigma}}_e = \widehat{\boldsymbol{\sigma}}_0 + \sum_{l=1}^{N} \left[\widehat{\mathbf{I}} + \widehat{\mathbf{p}}_l\right]^{-1} \left[\widehat{\mathbf{I}} - \Delta\widehat{\boldsymbol{\sigma}}_l^p \cdot \widehat{\boldsymbol{\Gamma}}_l\right]^{-1} \cdot \left[\widehat{\mathbf{I}} + \widehat{\mathbf{p}}_l\right] \cdot \Delta\widehat{\boldsymbol{\sigma}}_l f_l, \tag{3.53}$$

because $\Delta\widehat{\boldsymbol{\sigma}}_0 = 0$.

Note that, for heterogeneous media without polarizability, formula (3.53) corresponds to the Maxwell-Garnett theory of the composite geoelectrical medium (Choi, 1999).

The last formula provides a general solution of the effective conductivity problem for an arbitrary multi-phase composite polarized medium. This formula allows us to find the effective conductivity for inclusions with arbitrary shape and electrical properties. That is why the new composite geoelectrical model of the IP effect may be used to construct the effective conductivity for realistic rock formations typical for mineralization zones and/or petroleum reservoirs.

3.1.5 Effective resistivity of the isotropic medium filled with isotropic grains of arbitrary shape: anisotropy effect

We consider first a composite model with isotropic grains of arbitrary shape. In this case all conductivities become scalar functions:

$$\widehat{\boldsymbol{\sigma}}_0 = \widehat{\mathbf{I}}\sigma_0,\ \Delta\widehat{\boldsymbol{\sigma}}_l = \widehat{\mathbf{I}}\Delta\sigma_l,\ \Delta\widehat{\boldsymbol{\sigma}}_l^p = \left(\widehat{\mathbf{I}} + \widehat{\mathbf{p}}_l\right)\Delta\sigma_l$$

and, according to formula (3.30):

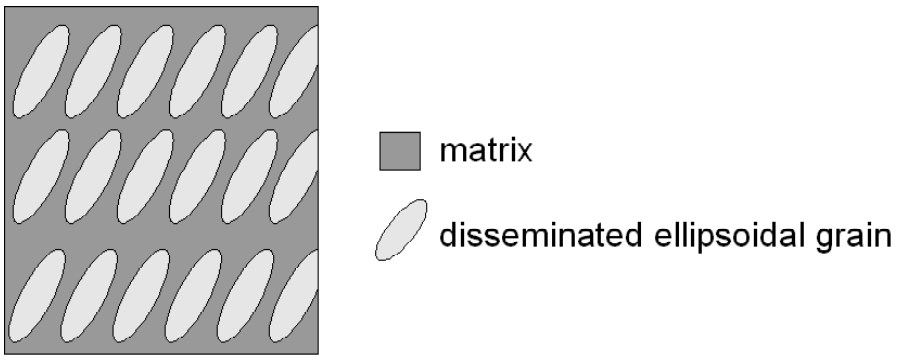

Figure 3-2 An example of electrically anisotropic media: a multi-phase model of the rock is composed of a set of ellipsoidal grains oriented in one direction .

$$\widehat{\mathbf{p}}_l = \xi_l \widehat{\mathbf{\Gamma}}_l^{-1} \cdot \widehat{\mathbf{\Lambda}}_l, \tag{3.54}$$

where ξ_l is equal to:

$$\xi_l = k_l \sigma_0 \sigma_l \left(\Delta\sigma_l\right)^{-1}. \tag{3.55}$$

Therefore, we can write:

$$\widehat{\boldsymbol{\sigma}}_e = \widehat{\boldsymbol{\sigma}}_b + \left\langle \left[\widehat{\mathbf{I}} + \widehat{\mathbf{p}}\right]^{-1} \widehat{\mathbf{q}} \right\rangle =$$

$$\widehat{\boldsymbol{\sigma}}_e = \widehat{\mathbf{I}}\sigma_0 + \sum_{l=1}^{N} \left[\widehat{\mathbf{I}} + \widehat{\mathbf{p}}_l\right]^{-1} \left[\widehat{\mathbf{I}} - \left(\widehat{\mathbf{I}} + \widehat{\mathbf{p}}_l\right) \Delta\sigma_l \widehat{\mathbf{\Gamma}}_l\right]^{-1} \left[\widehat{\mathbf{I}} + \widehat{\mathbf{p}}_l\right] \Delta\sigma_l f_l. \tag{3.56}$$

It can be demonstrated that, if the grains have nonisometric shape (e.g., ellipsoidal shape) but random orientation (see Figure 3-1), averaging of the tensor terms in expression (3.56) will result in scalarization. Therefore, the effective medium conductivity will become a scalar function. However, if all the grains are oriented in one specific direction as shown in Figure 3-2, the effective conductivity of this medium will become anisotropic. Thus, the effective conductivity may be a tensor in spite of the fact that the background medium and all the grains are electrically isotropic.

3.1.6 Fundamental IP model: effective resistivity of an isotropic multi-phase heterogeneous medium filled with spherical inclusions

It was demonstrated in the pioneer work of Pelton (1977), that the Cole-Cole relaxation model (Cole and Cole, 1941) can represent well the typical complex conductivity of polarized rock formations. In the framework of this model, the complex resistivity, $\rho\left(\omega\right)$, is described by the following well known expression:

$$\rho(\omega) = \rho\left(1 - \eta\left(1 - \frac{1}{1 + (i\omega\tau)^{\mathrm{C}}}\right)\right), \tag{3.57}$$

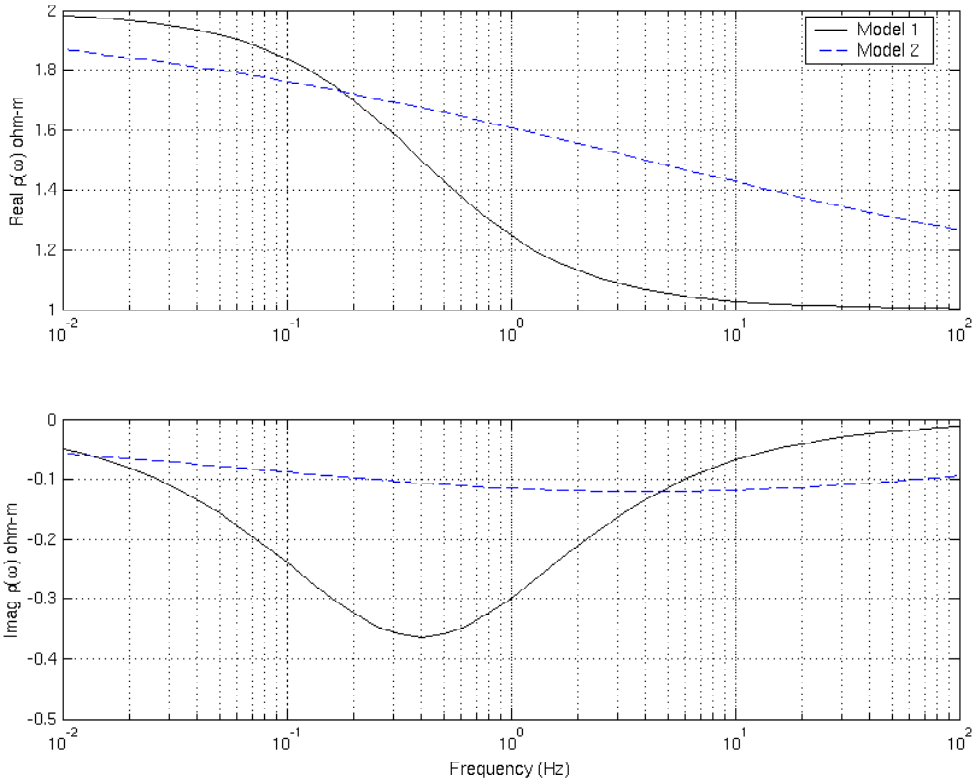

Figure 3-3 Examples of typical complex resistivity curves with the Cole-Cole model parameters. The upper panel shows the real part of the complex resistivity, while the bottom panel presents the imaginary part.

where ρ is the DC resistivity [Ohm-m]; ω is the angular frequency [rad/sec]; τ is the time parameter; η is the intrinsic chargeability (Seigel, 1959); and C is the relaxation parameter. The dimensionless intrinsic chargeability, η, characterizes the intensity of the IP effect.

Figure 3-3 presents examples of typical complex resistivity curves with the Cole-Cole model parameters defined according to the following table:

Table 1

	Model 1	Model 2
ρ_1	$= 2$ Ohm-m,	$\rho_2 = 2$ Ohm-m,
η_1	$= 0.5$,	$\eta_2 = 0.5$,
τ_1	$= 0.4$,	$\tau_2 = 0.04$,
C_1	$= 0.8$,	$C_2 = 0.3$.

One can see a significant difference between the solid and dashed curves in this plot, which corresponds to the different Cole-Cole models with different parameters.

Note also that the Cole-Cole curve gives us just one possible example of the relaxation model. There are several other models discussed in the geophysical literature (see, for example, Kamenetsky, 1997). One of the important practical questions is the relationship between the Cole-Cole model parameters and the petrophysical characteristics of mineralized rocks. There were several publications specifically dedicated to the solution of this problem. However, most of the published results provide just a qualitative indication of the correlation between the Cole-Cole parameters and specific mineralization characteristics of the rocks, such as mineral grain sizes and physical properties.

One of the reasons for electrical conductivity relaxation in rocks is the heterogeneity of formations containing microscopic inclusions of different minerals. In the pioneered work by Wait (1982, p.77), a simplified model of the composite medium as a loading of spherical conducting particles in a resistive background was introduced. The effective conductivity for this model was determined based on the equations of the static electric field. This model provided a foundation for the phenomenological theory of induced electrical polarization.

In this section we will show that Wait's model appears as a special case of the GEMTIP model, developed in this paper. We consider, as an example, an isotropic multi-phase composite model, with all model parameters described by the scalar functions. A composite model is formed by a homogeneous host medium of a volume V with a conductivity σ_0 filled with grains of spherical shape. We assume also that we have a set of N different types of grains, the lth grain type having radius a_l, conductivity σ_l, and surface polarizability k_l. In this model, both the volume and the surface depolarization tensors are constant scalar tensors equal to:

$$\widehat{\mathbf{\Gamma}}_l = \Gamma_l \widehat{\mathbf{I}} = -\widehat{\mathbf{I}} \frac{1}{3\sigma_b} \widehat{\mathbf{I}}, \quad \widehat{\mathbf{\Lambda}}_l = \Lambda_l \widehat{\mathbf{I}} = -\frac{2}{3\sigma_b a_l} \widehat{\mathbf{I}}. \tag{3.58}$$

The corresponding tensor formulas for conductivities, tensors $\widehat{\mathbf{m}}$ and $\widehat{\mathbf{q}}$, can be substituted by the scalar equations. For example, equation (3.45) for $\widehat{\mathbf{q}}$ takes the form:

$$q_l = \left[1 - \Delta\sigma_l^p \Gamma_l\right]^{-1} \Delta\sigma_l^p \left[1 - \Gamma_l \langle q \rangle\right], \tag{3.59}$$

and equation (3.35) for $\widehat{\mathbf{m}}$ becomes:

$$m_l = \left[1 + p_l\right]^{-1} q_l =$$

$$\left[1 - (1 + p_l)\, \Delta\sigma_l \Gamma_l\right]^{-1} \Delta\sigma_l \left[1 - \Gamma_l \langle q \rangle\right], \tag{3.60}$$

where, according to (3.30) and (3.21):

$$p_l = 2k_l a_l^{-1} \sigma_b \sigma_l \left(\Delta\sigma_l\right)^{-1}. \tag{3.61}$$

Formula (3.46) for $\langle \widehat{\mathbf{q}} \rangle$ is simplified, as well:

$$\langle q \rangle = \left\langle \left[1 - (1 + p_l)\,\Delta\sigma_l \Gamma_l\right]^{-1} \right\rangle^{-1} \left\langle \left[1 - (1 + p_l)\,\Delta\sigma_l \Gamma_l\right]^{-1} (1 + p_l)\,\Delta\sigma_l \Gamma_l \right\rangle. \tag{3.62}$$

In the framework of the self-consistent theory, the effective conductivity will be given by a scalar form of expression (3.52):

$$m_l = \left[1 - (1 + p_l)\,\Delta\sigma_l \Gamma_l\right]^{-1} \Delta\sigma_l. \tag{3.63}$$

Substituting formula (3.63) into (3.10), we obtain the following scalar formula for the effective conductivity of the polarized inhomogeneous medium:

$$\sigma_e = \sigma_b + \left\langle \left[1 - (1 + p_l)\,\Delta\sigma_l \Gamma_l\right]^{-1} \Delta\sigma_l \right\rangle =$$

$$\sigma_b + \left[1 - (1 + p_0)\,\Delta\sigma_0 \Gamma_0\right]^{-1} \Delta\sigma_0 f_0 + \sum_{l=1}^{N} \left[1 - (1 + p_l)\,\Delta\sigma_l \Gamma_l\right]^{-1} \Delta\sigma_l f_l. \tag{3.64}$$

In particular, assuming $\sigma_b = \sigma_0$ and, therefore, $\Delta\sigma_0 = 0$, we write:

$$\sigma_e = \sigma_0 + \sum_{l=1}^{N} \left[1 - (1 + p_l)\,\Delta\sigma_l \Gamma_l\right]^{-1} \Delta\sigma_l f_l. \tag{3.65}$$

Substituting expression (3.58) for the volume depolarization tensor and equation (3.63) for p_l, we finally find:

$$\sigma_e = \sigma_0 \left\{ 1 + 3 \sum_{l=1}^{N} \left[f_l \frac{\sigma_l - \sigma_0}{2\sigma_0 + \sigma_l + 2k_l a_l^{-1} \sigma_0 \sigma_l} \right] \right\}.$$

Multiplying the numerator and denominator by $\rho_l \rho_0$, (where $\rho_0 = 1/\sigma_0,\ \rho_l = 1/\sigma_l$), we obtain an equivalent expression for the effective resistivity of the composite polarized medium:

$$\rho_e = \rho_0 \left\{ 1 + 3 \sum_{l=1}^{N} \left[f_l \frac{\rho_0 - \rho_l}{2\rho_l + \rho_0 + 2k_l a_l^{-1}} \right] \right\}^{-1}. \tag{3.66}$$

It is well-known from the experimental data that the surface polarizability factor is a complex function of frequency. Let us represent the surface polarizability of the lth grain as:

$$k_l = b_l \left(i\omega\tau_l\right)^{-C_l}, \tag{3.67}$$

where:

$$b_l = a_l \left(2\rho_l + \rho_0\right)/2.$$

Therefore:

$$k_l = \frac{a_l}{2} \left(2\rho_l + \rho_0\right) \left(i\omega\tau_l\right)^{-C_l} \tag{3.68}$$

Thus, after some algebra, we have:

$$\rho_e = \rho_0 \left\{ 1 + \sum_{l=1}^{N} \left[f_l M_l \left[1 - \frac{1}{1 + (i\omega\tau_l)^{C_l}} \right] \right] \right\}^{-1}, \tag{3.69}$$

where:

$$M_l = 3\frac{\rho_0 - \rho_l}{2\rho_l + \rho_0}. \tag{3.70}$$

Note that, in the case of the metallic particles, one can assume that $\rho_l/\rho_0 \ll 1$, and we have:

$$M_l \approx 3. \tag{3.71}$$

Following Wait (1982), we adopt the model:

$$k_l = \alpha_l \left(i\omega\right)^{-C_l}, \tag{3.72}$$

which fits the experimental data, where α_l are some empirical surface polarizability coefficients, measured in the units $[\alpha_l] = (Ohm \times m^2) / \sec^{C_l}$.

Therefore from (3.72) and (3.68), we obtain:

$$\tau_l = \left[\frac{a_l}{2\alpha_l} \left(2\rho_l + \rho_0\right) \right]^{1/C_l}. \tag{3.73}$$

Formula (3.69) provides a general analytical expression for the effective conductivity of the multi-phase heterogeneous polarized medium, typical for mineralization zones.

In the case of a two-phase composite model, we have a homogeneous host medium of a volume V with a (complex) resistivity ρ_0 and spherical inclusions with the resistivity ρ_1. Formula (3.66) is simplified:

$$\rho_e = \rho_0 \left\{ 1 + f_1 M_1 \left[1 - \frac{1}{1 + (i\omega\tau_1)^{C_1}} \right] \right\}^{-1}. \tag{3.74}$$

After some algebra, we arrive at the conventional Cole-Cole formula for the effective resistivity:

$$\rho_e = \rho_0 \left\{ 1 - \eta \left[1 - \frac{1}{1 + (i\omega\tau)^{C}} \right] \right\}, \tag{3.75}$$

where:

$$\eta = \frac{3f_1 \left(\rho_0 - \rho_1\right)}{2\rho_1 + \rho_0 + 3f_1 \left(\rho_0 - \rho_1\right)}, \tag{3.76}$$

and

$$\tau = \left[\frac{a_1}{2\alpha_1} \left(2\rho_1 + \rho_0 + 3f_1 \left(\rho_0 - \rho_1\right)\right) \right]^{1/C}. \tag{3.77}$$

Note that in formula (3.75) we use the same notations as in the original Cole-Cole formula (3.57).

Finally, let us assume that $\rho_1/\rho_0 \ll 1$, which is typical for metallic particles, for example. Than we have:

$$\eta = \frac{3f_1}{1+3f_1}. \tag{3.78}$$

In particular, if the volume fraction of the metallic particles is very small, we obtain:

$$\eta \approx 3f_1. \tag{3.79}$$

3.2 Development of the 3-D EM-IP forward modeling system

Traditionally, electromagnetic (EM) modeling has been based on geoelectrical models of geological targets (e.g., ore deposits), which are characterized by some bulk conductivity distribution described by a real function of the spatial coordinates. It is also usually assumed that the conductivity is time and/or frequency independent. However, the actual conductivity of geological formations is defined by the complex microscopic and macroscopic heterogeneous structures of minerals and rocks with different petrophysical properties. This intrinsic complexity of the internal structure of the rocks may result in complex values of the bulk conductivity. Moreover, this complexity may give rise to frequency and/or time dependence of the rock's conductivity, which is manifested through IP effects.

In this research project we have developed an approach to constructing a new generation of EM modeling software which takes into account the true complexity of the rocks. Our approach is based on the rock physics description of the medium as a composite heterogeneous multiphase formation. We have developed a generalized effective-medium theory of induced polarization (GEMTIP) to generate effective conductivity models of an ore deposit. Our new formulation of a geoelectrical model takes into account the mineralization and/or fluid content of the rocks and the matrix composition, porosity, anisotropy, and polarizability of the formations. This approach allows us to provide a link between the volume content of the different minerals and the observed EM field data, which is an important goal of this project.

For modeling an IP response in the frequency domain, i.e., spectral IP modeling, we need to solve the Maxwell's equations for the complex conductivity model. Using this modeling method, we can investigate the effect of different complex conductivity relaxation models, including the Cole-Cole model and a composite GEMTIP model, and we can obtain the EM responses for the various types of transmitting sources including the current bipoles used in conventional IP surveys.

During the first two years of the project we have developed a prototype of 3-D IP modeling algorithm using the integral equation (IE) method. Our IE forward modeling code INTEM3DIP is based on the contraction IE method, which improves the convergence rate of the iterative solvers (Hursán and Zhdanov, 2002). This code can handle various types of sources and receivers to compute the effect of the complex resistivity model. In addition, the preprocessing and postprocessing routines are developed to obtain conventional IP responses as well. We have tested the working version of the INTEM3DIP code for computer simulation of the IP data for several models including the southwest US porphyry model and the Kambalda-style nickel sulfide deposit in Australia. The results of this modeling study are presented below.

3.2.1 Formulation of the integral equation (IE) method

We consider, first, the basic integral equations of 3-D EM forward modeling, written for the total electric $\mathbf{E}$ and magnetic $\mathbf{H}$ fields:

$$\mathbf{E}(\mathbf{r}') = \iiint_D \widehat{\mathbf{G}}_E(\mathbf{r}' \mid \mathbf{r}) \cdot [\Delta\widetilde{\sigma}(\mathbf{r})\mathbf{E}(\mathbf{r})]\, dv + \mathbf{E}^b(\mathbf{r}')$$

$$= \mathbf{G}_E[\Delta\widetilde{\sigma}(\mathbf{r})\mathbf{E}(\mathbf{r})] + \mathbf{E}^b(\mathbf{r}'), \tag{3.80}$$

$$\mathbf{H}(\mathbf{r}') = \iiint_D \widehat{\mathbf{G}}_H(\mathbf{r}' \mid \mathbf{r}) \cdot [\Delta\widetilde{\sigma}(\mathbf{r})\mathbf{E}(\mathbf{r})]\, dv + \mathbf{H}^b(\mathbf{r}')$$

$$= \mathbf{G}_H[\Delta\widetilde{\sigma}(\mathbf{r})\mathbf{E}(\mathbf{r})] + \mathbf{H}^b(\mathbf{r}'), \tag{3.81}$$

where $\widehat{\mathbf{G}}_E(\mathbf{r}_j \mid \mathbf{r})$ and $\widehat{\mathbf{G}}_H(\mathbf{r}_j \mid \mathbf{r})$ are the electric and magnetic Green's tensors defined for an unbounded conductive medium with the complex background conductivity $\widetilde{\sigma}_b$; $\mathbf{G}_E$ and $\mathbf{G}_H$ are corresponding Green's linear operators; and $\mathbf{E}^b$, $\mathbf{H}^b$ are the background electric and magnetic fields; domain D corresponds to the volume with the complex anomalous conductivity distribution $\widetilde{\sigma}(\mathbf{r}) = \widetilde{\sigma}_b + \Delta\widetilde{\sigma}(\mathbf{r})$, $\mathbf{r} \in D$.

Equation (3.80) written for the points $\mathbf{r}'$ located inside domain D, $\mathbf{r}' \in D$, gives us an integral equation with respect to electric field $\mathbf{E}(\mathbf{r})$. The main problem is to solve this integral equation.

The conventional approach to discretization of the integral equation (3.80) is based on dividing domain D into N elementary cells, D_n, formed by some rectangular grid in the domain $D = \bigcup_{n=1}^{N} D_n$, and assuming that $\Delta\widetilde{\sigma}(\mathbf{r})$ has the constant value $\Delta\widetilde{\sigma}_n$ within a cell. Note that the coefficients $\Delta\widetilde{\sigma}_n$ can be represented as the components of a vector $\boldsymbol{\sigma}$ of the order N:

$$\boldsymbol{\sigma} = [\Delta\widetilde{\sigma}_1, \Delta\widetilde{\sigma}_2, ..., \Delta\widetilde{\sigma}_N]^T,$$

where superscript "T" denotes transposition.

We also assume that each cell D_n is so small that the electric field is approximately constant within the cell, $\mathbf{E}(\mathbf{r}) \approx \mathbf{E}(\mathbf{r}_n)$, where $\mathbf{r}_n$ is a center point of rectangular cell D_n. Under this condition, equation (3.80) takes the form:

$$\mathbf{E}(\mathbf{r}_p) = \sum_{n=1}^{N} \iiint_{D_n} \widehat{\mathbf{G}}_E(\mathbf{r}_p \mid \mathbf{r})\, dv \cdot \Delta\widetilde{\sigma}_{\mathbf{n}} \mathbf{E}(\mathbf{r}_n) + \mathbf{E}^b(\mathbf{r}_p), \quad p = 1, 2, ...N. \tag{3.82}$$

Thus, inside the anomalous domain D, the discrete analog of equation (3.80) can be written as (Zhdanov, 2002):

$$\mathbf{e}_D = \widehat{\mathbf{G}}_D \widehat{\boldsymbol{\sigma}} \mathbf{e}_D + \mathbf{e}_D^b, \tag{3.83}$$

where $\widehat{\boldsymbol{\sigma}}$ is a $(3N \times 3N)$ diagonal matrix of anomalous conductivities:

$$\widehat{\boldsymbol{\sigma}} = \begin{bmatrix} \Delta\widetilde{\sigma}_1 & \cdots & 0 & 0 & \cdots & 0 & 0 & \cdots & 0 \\ & & & & \vdots & & & & \\ 0 & \cdots & \Delta\widetilde{\sigma}_N & 0 & \cdots & 0 & 0 & \cdots & 0 \\ 0 & \cdots & 0 & \Delta\widetilde{\sigma}_1 & \cdots & 0 & 0 & \cdots & 0 \\ & & & & \vdots & & & & \\ 0 & \cdots & 0 & 0 & \cdots & \Delta\widetilde{\sigma}_N & 0 & \cdots & 0 \\ 0 & \cdots & 0 & 0 & \cdots & 0 & \Delta\widetilde{\sigma}_1 & \cdots & 0 \\ & & & & \vdots & & & & \\ 0 & \cdots & 0 & 0 & \cdots & 0 & 0 & \cdots & \Delta\widetilde{\sigma}_N \end{bmatrix}, \tag{3.84}$$

$\mathbf{e}_D$ and $\mathbf{e}_D^b$ are the vectors of the total and background electric fields formed by the x, y and z components of these fields at the centers of the cells D_n of the anomalous domain D:

$$\mathbf{e}_D = [E_x^1, E_x^2, ...E_x^N, E_y^1, E_y^2, ...E_y^N, E_z^1, E_z^2, ...E_z^N]^T,$$

$$\mathbf{e}_D^b = [E_x^{b,1}, E_x^{b,2}, ...E_x^{b,N}, E_y^{b,1}, E_y^{b,2}, ...E_y^{b,N}, E_z^{b,1}, E_z^{b,2}, ...E_z^{b,N}]^T.$$

These vectors have the order $3N$.

The $3N \times 3N$ matrix $\widehat{\mathbf{G}}_D$ is formed by the volume integrals over the elementary cells D_n of the components of the corresponding electric Green's tensor $\widehat{\mathbf{G}}_E$, acting inside domain D :

$$\widehat{\mathbf{G}}_D = \begin{bmatrix} G_{xx}^{11} & \cdots & G_{xx}^{1N} & G_{xy}^{11} & \cdots & G_{xy}^{1N} & G_{xz}^{11} & \cdots & G_{xz}^{1N} \\ & & & & \vdots & & & & \\ G_{xx}^{N1} & \cdots & G_{xx}^{NN} & G_{xy}^{N1} & \cdots & G_{xy}^{NN} & G_{xz}^{N1} & \cdots & G_{xz}^{NN} \\ G_{yx}^{11} & \cdots & G_{yx}^{1N} & G_{yy}^{11} & \cdots & G_{yy}^{1N} & G_{yz}^{11} & \cdots & G_{yz}^{1N} \\ & & & & \vdots & & & & \\ G_{yx}^{N1} & \cdots & G_{yx}^{NN} & G_{yy}^{N1} & \cdots & G_{yy}^{NN} & G_{yz}^{N1} & \cdots & G_{yz}^{NN} \\ G_{zx}^{11} & \cdots & G_{zx}^{1N} & G_{zy}^{11} & \cdots & G_{zy}^{1N} & G_{zz}^{11} & \cdots & G_{zz}^{1N} \\ & & & & \vdots & & & & \\ G_{zx}^{N1} & \cdots & G_{zx}^{NN} & G_{zy}^{N1} & \cdots & G_{zy}^{NN} & G_{zz}^{N1} & \cdots & G_{zz}^{NN} \end{bmatrix}, \tag{3.85}$$

where:

$$G^{pn}_{\alpha\beta} = \iiint_{D_n} G_{E\alpha\beta}\left(\mathbf{r}_p \mid \mathbf{r}\right) dv,\ \alpha,\beta = x,y,z;\ p,n = 1,2,...N.$$

Thus, forward EM modeling based on the IE method is reduced to the solution of the matrix equation (3.83) in the unknown vector $\mathbf{e}_D$ of the electric field components inside domain D. The equation is a $3N \times 3N$ linear system,

$$\widehat{\mathbf{A}}\mathbf{e}_D = \mathbf{e}^b_D, \tag{3.86}$$

where

$$\widehat{\mathbf{A}} = \widehat{\mathbf{I}} - \widehat{\mathbf{G}}_D\widehat{\boldsymbol{\sigma}}. \tag{3.87}$$

Matrix $\widehat{\mathbf{A}}$ is a $3N \times 3N$ dense matrix. One can use different types of iterative methods, discussed in Zhdanov (2002), for the solution of this problem.

3.2.2 3-D EM forward modeling based on the contraction integral equation method

It was demonstrated in Zhdanov (2002) that one can apply a special linear transformation to the Green's operator to obtain a new modified Green's operator, $\mathbf{G}^m_E$, with norm less than one. As a result, the original integral equation (3.80) can be converted into a contraction operator-based equation:

$$a\mathbf{E}^a + b\mathbf{E}^b = \mathbf{G}^m_E\left[b(\mathbf{E}^a + \mathbf{E}^b)\right], \tag{3.88}$$

where:

$$a = \frac{2\sigma_b + \Delta\widetilde{\sigma}}{2\sqrt{\sigma_b}},\ b = \frac{\Delta\widetilde{\sigma}}{2\sqrt{\sigma_b}}, \tag{3.89}$$

and operator $\mathbf{G}^m_E(\mathbf{x})$ is defined as a linear transformation of the original electric Green's operator:

$$\mathbf{G}^m_E(\mathbf{x}) = \sqrt{\sigma_b}\mathbf{G}_E\left(2\sqrt{\sigma_b}\mathbf{x}\right) + \mathbf{x}. \tag{3.90}$$

Using the original Green's operator given by expression (3.80) and taking into account formula (3.90), one can rewrite equation (3.88) as follows:

$$\sqrt{\sigma_b}a^{-1}\widetilde{\mathbf{E}} - \sqrt{\sigma_b}\mathbf{G}_E\left(\Delta\widetilde{\sigma}a^{-1}\widetilde{\mathbf{E}}\right) = \sqrt{\sigma_b}\mathbf{E}^b. \tag{3.91}$$

This is the basic equation of the CIE method of EM modeling.

The contraction integral equation (3.91) can be treated as the preconditioned conventional integral equation (3.86) (Zhdanov, 2002; Hursan and Zhdanov, 2002). Indeed, in discrete form, equation (3.91) can be written as:

$$\widehat{\mathbf{M}}_1\left(\widehat{\mathbf{I}} - \widehat{\mathbf{G}}_D\widehat{\boldsymbol{\sigma}}\right)\widehat{\mathbf{M}}_2\widetilde{\mathbf{e}}_D = \widehat{\mathbf{M}}_1\mathbf{e}^b_D, \tag{3.92}$$

where $\widehat{\mathbf{M}}_1$ is the left preconditioner, and $\widehat{\mathbf{M}}_2$ is the right preconditioner, and

$$\widetilde{\mathbf{e}}_D = \widehat{\mathbf{M}}^{-1}_2\mathbf{e}_D. \tag{3.93}$$

The preconditioners $\widehat{\mathbf{M}}_1$ and $\widehat{\mathbf{M}}_2$ are the $3N \times 3N$ diagonal matrices, similar to matrix (3.84):

$$\widehat{\mathbf{M}}_1 = \mathbf{diag}\left(\sqrt{\sigma_1^b}, \sqrt{\sigma_2^b}, ..., \sqrt{\sigma_N^b}, \sqrt{\sigma_1^b}, \sqrt{\sigma_2^b}..., \sqrt{\sigma_N^b}, \sqrt{\sigma_1^b}, \sqrt{\sigma_2^b}..., \sqrt{\sigma_N^b}\right),$$

$$\widehat{\mathbf{M}}_2 = \mathbf{diag}\left(a_1^{-1}, a_2^{-1}, ..., a_N^{-1}, a_1^{-1}, a_2^{-1}, ..., a_N^{-1}, a_1^{-1}, a_2^{-1}, ..., a_N^{-1}\right), \tag{3.94}$$

where, according to (3.89):

$$a_i = \frac{2\sigma_{bi} + \Delta\widetilde{\sigma}_i}{2\sqrt{\sigma_{bi}}},\ i = 1, 2, ..., N.$$

Finally, we can write equation (3.92) in the form:

$$\mathbf{f} = \widehat{\mathbf{L}}\mathbf{m}, \tag{3.95}$$

where:

$$\widehat{\mathbf{L}} = \widehat{\mathbf{M}}_1\left(\widehat{\mathbf{I}} - \widehat{\mathbf{G}}_D\widehat{\boldsymbol{\sigma}}\right)\widehat{\mathbf{M}}_2,\ \mathbf{f} = \widehat{\mathbf{M}}_1\mathbf{e}_D^b,\ \text{and}\ \mathbf{m} = \widetilde{\mathbf{e}}_D. \tag{3.96}$$

3.2.3 The generalized minimal residual method

We use the complex generalized minimal residual method (CGMRM) to solve the linear system of equations (3.95). The preconditioning speeds up the solution of IE (3.86) significantly.

Let us consider a general linear operator equation:

$$\mathbf{f} = L\mathbf{m}, \tag{3.97}$$

where $\mathbf{f}, \mathbf{m} \in M$, and L is a linear continuous operator in M. We assume also that M is a complex Hilbert space.

The general iterative solution of equation (3.97) can be expressed by the formula:

$$\mathbf{m}_{n+1} = \mathbf{m}_n + \Delta\mathbf{m}_n = \mathbf{m}_n - k_n\mathbf{r}_n,\ n = 0, 1, 2, ... \tag{3.98}$$

where $\mathbf{m}_0$ is some initial approximation, $\Delta\mathbf{m}_n$ is an iteration step:

$$\Delta\mathbf{m}_n = -k_n\mathbf{r}_n, \tag{3.99}$$

$\mathbf{r}_n$ is a residual on the n-th step,

$$\mathbf{r}_n = L\mathbf{m}_n - \mathbf{f}, \tag{3.100}$$

and k_n is an iteration coefficient. Note that the residual on the $(n+1)$-th step, $\mathbf{r}_{n+1}$, is related to $\mathbf{r}_n$ by the formula:

$$\mathbf{r}_{n+1} = L\mathbf{m}_{n+1} - \mathbf{f} = L\mathbf{m}_n - k_nL\mathbf{r}_n - \mathbf{f} = \mathbf{r}_n - k_nL\mathbf{r}_n. \tag{3.101}$$

An obvious choice for the iteration coefficient k_n is to minimize the norm of the residual $\mathbf{r}_{n+1}$:

$$\|\mathbf{r}_{n+1}\|^2 = \|\mathbf{r}_n - k_n L\mathbf{r}_n\|^2 = \Phi^2(k_n) = \min. \tag{3.102}$$

An expression for the value of k_n that minimizes $\|\mathbf{r}_{n+1}\|^2$ has the form (Zhdanov, 2002):

$$k_n = \frac{(\mathbf{r}_n, L\mathbf{r}_n)}{(L\mathbf{r}_n, L\mathbf{r}_n)}. \tag{3.103}$$

An effective method to accelerate the convergence of the MRM algorithm is based on the Krylov-subspace, which is the finite dimensional subspace K_s of the Hilbert space M, spanned by the vectors $\mathbf{r}_n, L\mathbf{r}_n, L^2\mathbf{r}_n, ...L^{q-1}\mathbf{r}_n$:

$$K_s = \text{span}\left\{\mathbf{r}_n, L\mathbf{r}_n, L^2\mathbf{r}_n, ...L^{q-1}\mathbf{r}_n\right\}.$$

The CGMRM method is based on introducing an orthogonal basis $\left\{L\mathbf{g}_1^{(n)}, L\mathbf{g}_2^{(n)}, ..., L\mathbf{g}_s^{(n)}\right\}$ in the subspace K_s' spanned by the vectors $\left\{L\mathbf{r}_n, L^2\mathbf{r}_n, ...L^q\mathbf{r}_n\right\}$ and finding the coefficients k_{nl} as projections of the residual $\mathbf{r}_n$ on the vectors from this basis (Zhdanov, 2002). The algorithm of the CGMRM can be summarized as follows:

$$\begin{aligned}
&\mathbf{r}_n = L\mathbf{m}_n - \mathbf{f}, \quad \mathbf{g}_1^{(n)} = \mathbf{r}_n, \quad \mathbf{r}_{n+1,(1)} = \mathbf{r}_n - k_{n1}L\mathbf{g}_1^{(n)}, && (a)\\
&\mathbf{r}_{n+1,(p)} = \mathbf{r}_{n+1,(p-1)} - k_{np}L\mathbf{g}_p^{(n)}, && (b)\\
&\mathbf{g}_p^{(n)} = \mathbf{r}_{n+1,(p-1)} - \textstyle\sum_{l=1}^{p-1}\beta_{pl}^{(n)}\mathbf{g}_l^{(n)}, \quad p = 2,3,...s, && (c)\\
&\beta_{pl}^{(n)} = \left(L\mathbf{r}_{n+1,(p-1)}, L\mathbf{g}_l^{(n)}\right) / \left\|L\mathbf{g}_l^{(n)}\right\|^2, \quad k_{np} = \left(\mathbf{r}_n, L\mathbf{g}_p^{(n)}\right) / \left\|L\mathbf{g}_p^{(n)}\right\|^2, && (d)\\
&\mathbf{m}_{n+1} = \mathbf{m}_n - \textstyle\sum_{l=1}^{s} k_{nl}\mathbf{g}_l^{(n)}, \quad n = 1,2,3,..... && (e)
\end{aligned} \tag{3.104}$$

The iterative process (3.104) is terminated when the misfit reaches the given level ε_0 :

$$\|\mathbf{r}_N\|^2 \leq \varepsilon_0.$$

The main advantage of the CGMRM method is that there exists a convergence theorem for this iterative method. It states that the generalized minimal residual method, based on the recursive formulae (3.104), converges to the solution of the linear operator equation (3.97) for any initial approximation $\mathbf{m}_0$, if L is an absolutely positively determined (APD) linear continuous operator, acting in a complex Hilbert space M (Zhdanov, 2002).

4. EXPERIMENTAL

4.1 Kambalda-style nickel sulfide deposit

In order to illustrate the capability of the developed forward method and software, we have computer simulated the EM-IP response for a model of the Kambalda-style nickel sulfide deposit in Australia. In tropical and arid terrains such as Australia and southern Africa, the differential weathering characteristics of the near-surface rock units comprising the regolith often result in large lateral changes in the overburden conductivity. In the general exploration model, the regolith is highly conductive and overlays the resistive host rock and conductive target. To the explorer trying to use EM methods, this inhomogeneous regolith creates "false" anomalies due to conductive sedimentary and weathered units, and the extensive blanket of salt lake sediments in certain areas effectively masks the EM response from the target (e.g., McCracken et al., 1986). All these factors point towards the associated analysis of EM-IP responses being an extremely challenging problem.

To demonstrate the effectiveness of our modeling software, we simulated an IP survey above a stratiform komatiitic peridiotite-hosted (Type 1A), or Kambalda-style, nickel sulfide deposit located beneath a complicated regolith horizon. As described by Stone and Masterman (1998), Kambalda-style orebodies occur at, or close to, the basal contact between the lowermost komatiite flow (ultramafic) and footwall metabasalts (mafic). The NiS ore is comprised of basal massive, matrix and disseminated sulfide ores within which the nickel grade decreases upward. Strike lengths of the orebodies vary between 50 m and 350 m for mineralized widths of 5 m to 20 m.

As discussed in detail by Trench and Williams (1994), potentially all geophysical techniques have application for the direct exploration of nickel sulfide (NiS) deposits. For EM methods, Kambalda-style models have been the subject of previous 3-D EM forward modeling studies such as Stolz et al. (1995) and Zhdanov et al. (2000). However, there are specific limitations on EM methods for the practical exploration of Kambalda-style NiS exploration in Australia and these are imposed by the following factors (Trench and Williams, 1994):

a) the generally small size of the deposits (0.5 to 3.0 Mt);

b) the extreme depth of weathering in the regolith; and

c) the abundance of anomalous responses from noneconomic targets.

We base the petrophysical characteristics of the Kambalda-style model on those electrical parameters described by Trench and Williams (1994). The surficial alluvial layer of the regolith is 12.5 m thick and has a conductivity of 0.05 S/m. This overlies a weathered basalt layer of 40 m thickness and a

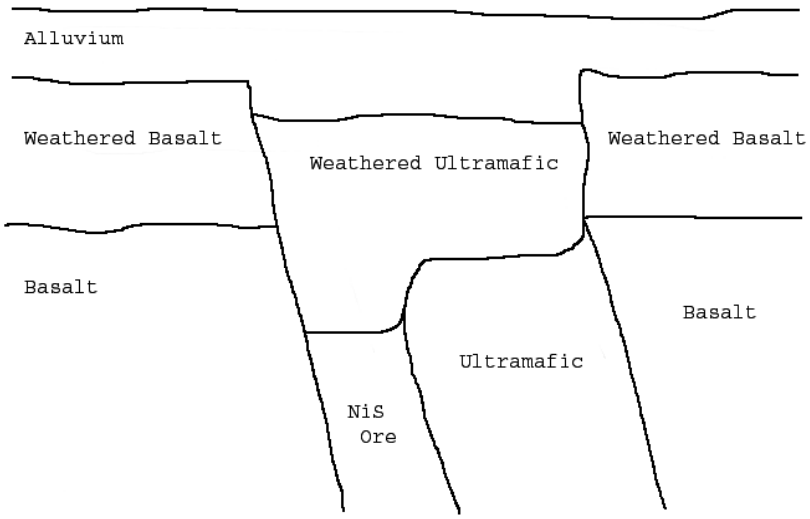

Figure 4-1 Cartoon of the cross-section of the Kambalda NiS deposit after Trench and Williams (1994).

conductivity of 0.01 S/m. This regolith overlies a resistive basalt host rock of 0.001 S/m. Differential weathering of the ultramafic host of the NiS mineralization in the regolith is extended at depth into the basalt host rock. This weathered ultramafic has a conductivity of 0.05 S/m. The NiS ore, with a conductivity of 1 S/m, and an unweathered ultramafic mineralization host with a conductivity of 0.01 S/m, extend at depth and with steep dip beneath the weathered ultramafic host. The NiS ore and ultramafic host have a 700 m strike length in the x direction. Figure 4-1 is a cartoon of the cross-section of the Kambalda deposit from Trench and Williams (1994). Figure 4-2 presents a resistivity cross-section of the Kambalda-style model studied in this paper along the profile $y = 0$ m.

We have designed various models based on a single initial model of the Kambalda deposit, presented in Figure 4-2, to test the usability of the software and to catalog the modeling results. Four separate forward modeling runs using INTEM3DIP were executed based on varying parameters of the ore body and background resistivities. All models show a horizontal 3-layered background with varying thicknesses but fixed resistivities and IP phases of [20, 100, 1000] Ohm-m and [5, 10, 5] mrad respectively. The overlying weathered ultramafic and adjacent ultramafic bodies were each given resistivities and IP phases of [20, 100] Ohm-m and [5, 20] mrad. Similar EM properties of the ore body are [10] Ohm-m and [100] mrad.

The forward modeling results are presented as apparent resistivity/phase pseudosections below.

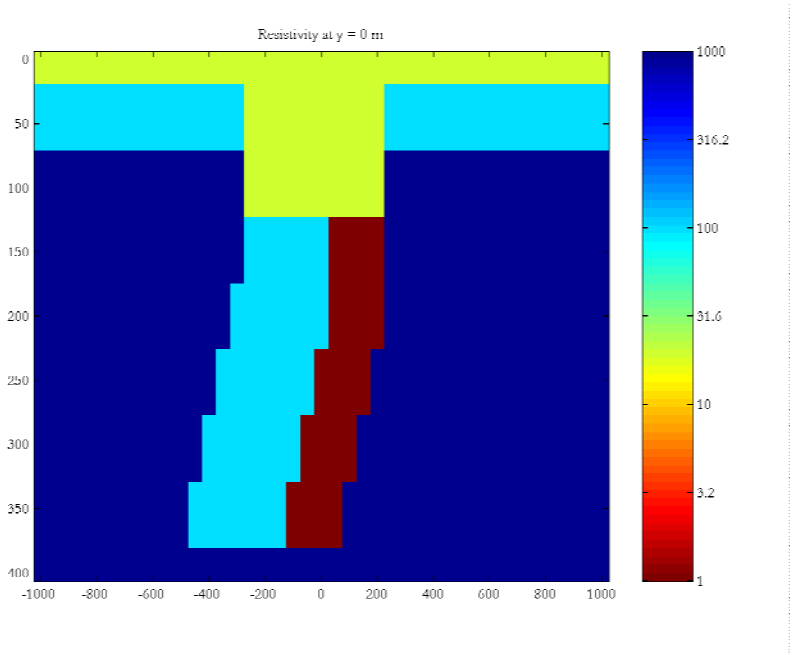

Figure 4-2 Cross-section of the total resistivity along the $y = 0$ m profile for the Kambalda-style NiS ore body used for forward modeling the FEM response.

4.1.1 Trench-Williams Model 1 (TWM1)

The initial model TWM1 was created from Figure 4-2, where the slanting of the ore body was represented by hexagons shifted with increasing depth. The vertical and longitudinal dimensions of the ore body were 250 m and 600 m respectively with a thickness of 200 m. Model TWM1 is the basis model for the modeling surveys. The latter models show increased ore deposit geometries to analyze output effects.

A 3-D view of this model is shown in Figure 4-3, while Figure 4-4 presents the pseudosections of apparent resistivity and phase for this model. These pseudosections provide a very complex image of the deposit, which is difficult to interpret without using an appropriate inversion method. Nevertheless, we can clearly see both the anomalous resistivity and IP effects in these sections.

4.1.2 Trench-Williams Model 2 (TWM2)

Model TWM2 is a manipulated version of TWM1 where the dx, dy, dz discretization has been increased to 50 m instead of 25 m and the layer thicknesses have been increased (Figure 4-5). These changes were made to facilitate computation "run time" and to slightly increase the depth of the ore body. The vertical and longitudinal dimensions of the ore body were 250 m and 600 m

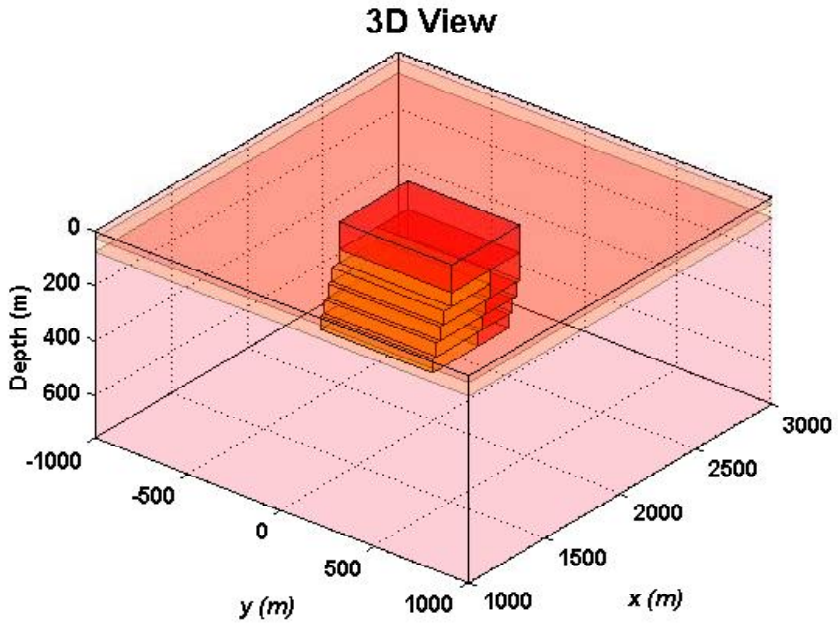

Figure 4-3 A 3-D view of Trench-Williams Model 1 (TWM1).

respectively with a thickness of 250 m.

The pseudosections (Figure 4-6) are very similar to those for model TWM1, but with softer contrasts from the edge effects, particularly in the apparent resistivity plot.

4.1.3 Trench-Williams Model 3 (TWM3)

Model TWM3 has extended the ore deposit length from TWM2 by 100 m in both positive and negative y-directions (Figure 4-7). The upper two background layer thicknesses have also been doubled to 50 m and 100 m. The vertical and longitudinal dimensions of the ore body were 250 m and 800 m respectively with a thickness of 250 m.

As the model size has been increased, it has become easier to facilitate computation as well as 3D visualization.

The pseudosection plots are reappearing in similar patterns, though, with introduced heterogeneities, particularly in the apparent resistivity plots (Figure 4-8). Note also that the edge effects are decreasing with larger geometries.

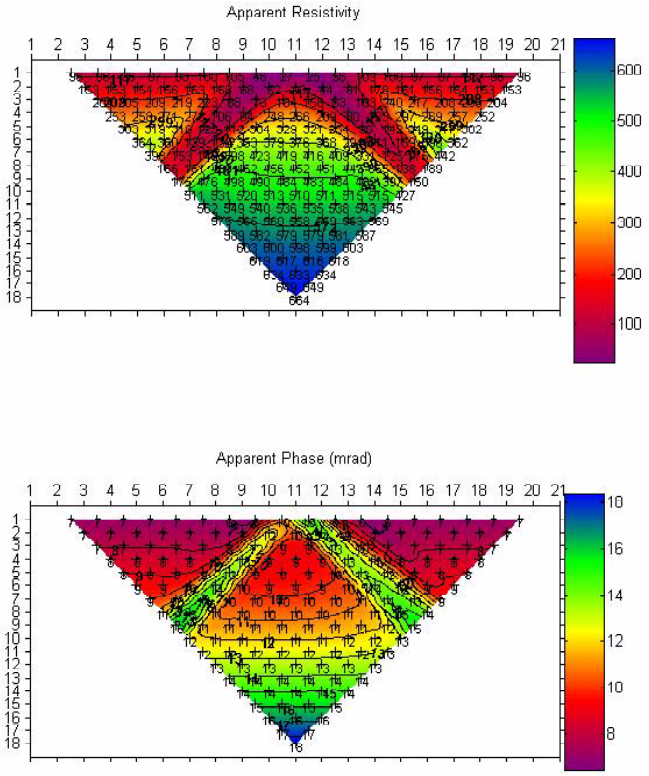

Figure 4-4 Pseudosections of apparent resistivity and phase for Trench-Williams Model 1.

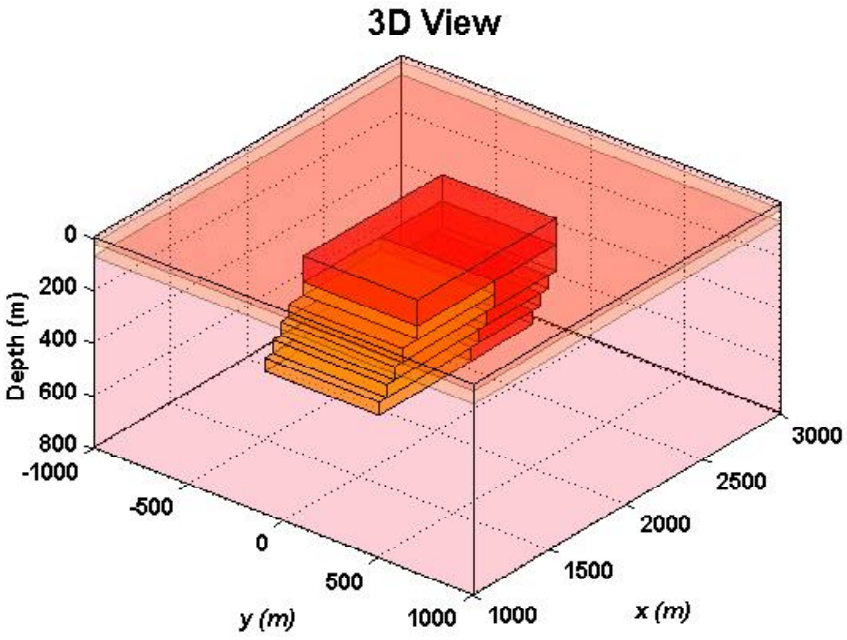

Figure 4-5 A 3-D view of Trench-Williams Model 2 (TWM2).

4.1.4 Trench-Williams Model 4 (TWM4)

Finally, model TWM4 was created with an interest in analyzing effects from an over-exaggerated model in depth (Figure 4-9). Though this model does not hold with the geometric parameters as set for in the original model, it was created with the intent of comparing these results with those of the smaller, more correct, models. The vertical and longitudinal thicknesses of the ore body were 500 m and 1000 m respectively with a thickness of 250 m.

The depth of the lowermost layer in the ore deposit is at 650m. Computational "run time" was greatest for this particular model.

Figure 4-10 presents the corresponding pseudosection plots, computed for model TWM4. They show similar results as before, only here, the larger increase in apparent phase (as shown in blue) provided indication that the geometry of the ore deposit was resistively favored to one side. Model TWM1 showed this same phenomenon, but with a smaller phase contrast.

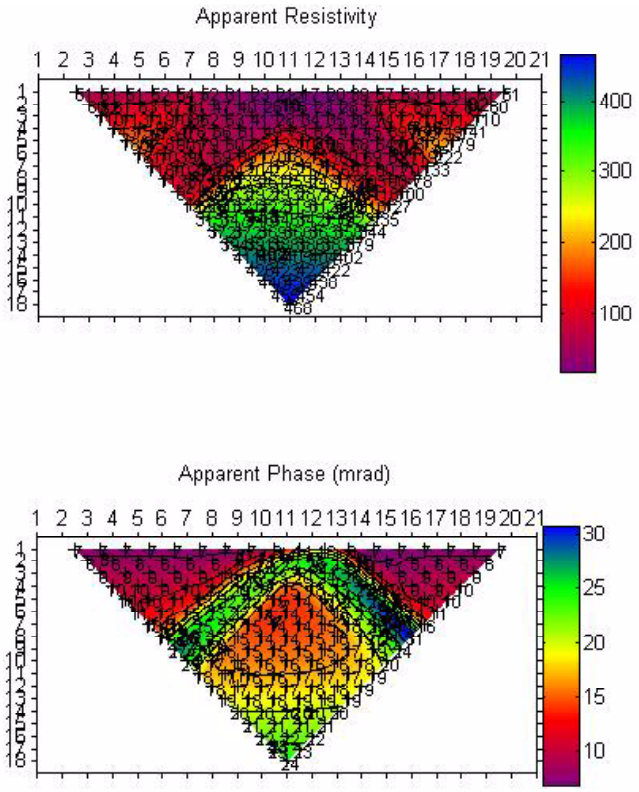

Figure 4-6 Pseudosections of apparent resistivity and phase for Trench-Williams Model 2.

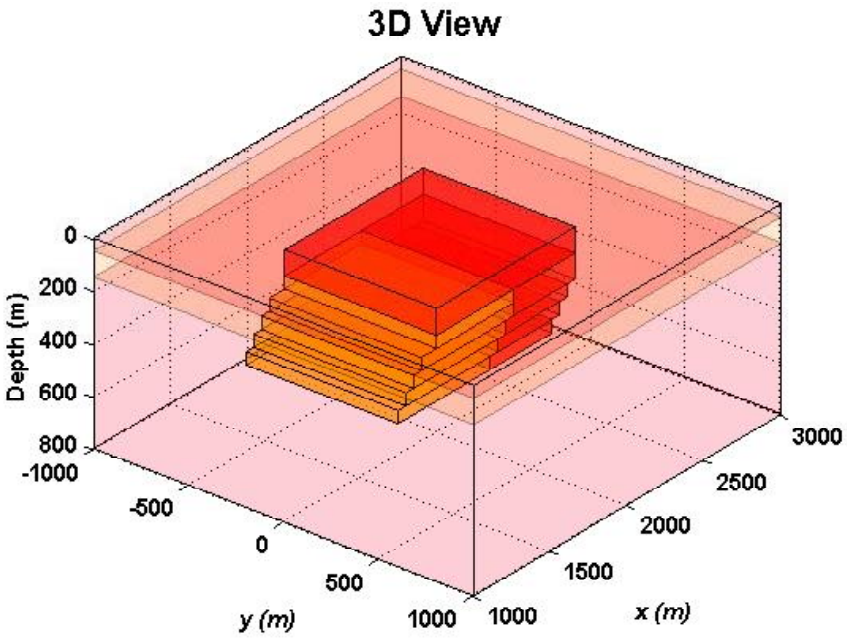

Figure 4-7 A 3-D view of Trench-Williams Model 3 (TWM3).

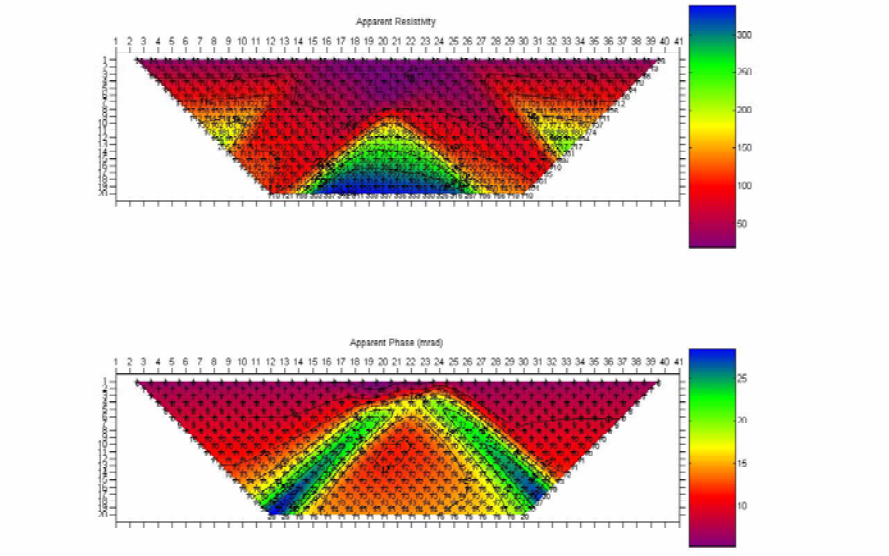

Figure 4-8 Pseudosections of apparent resistivity and phase for Trench-Williams Model 3.

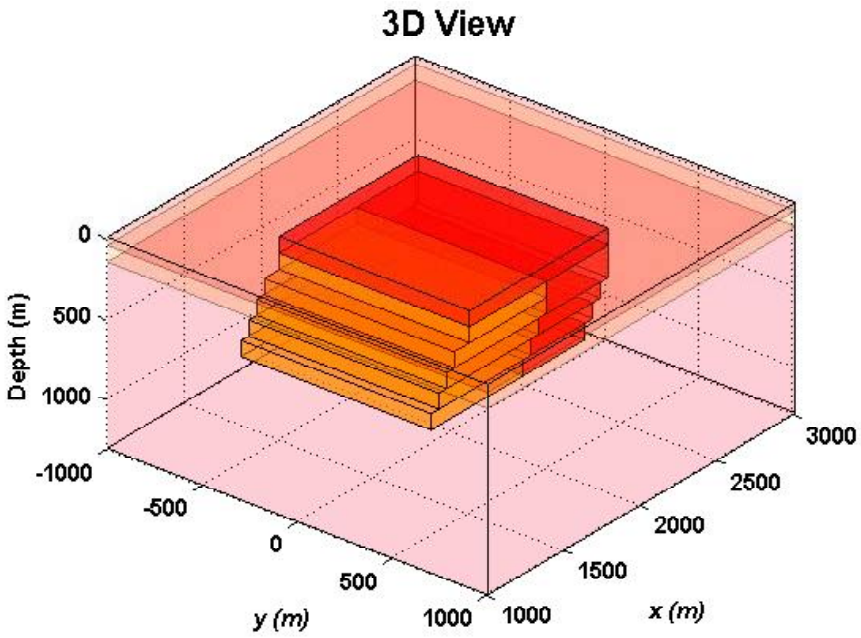

Figure 4-9 A 3-D view of Trench-Williams Model 4 (TWM4).

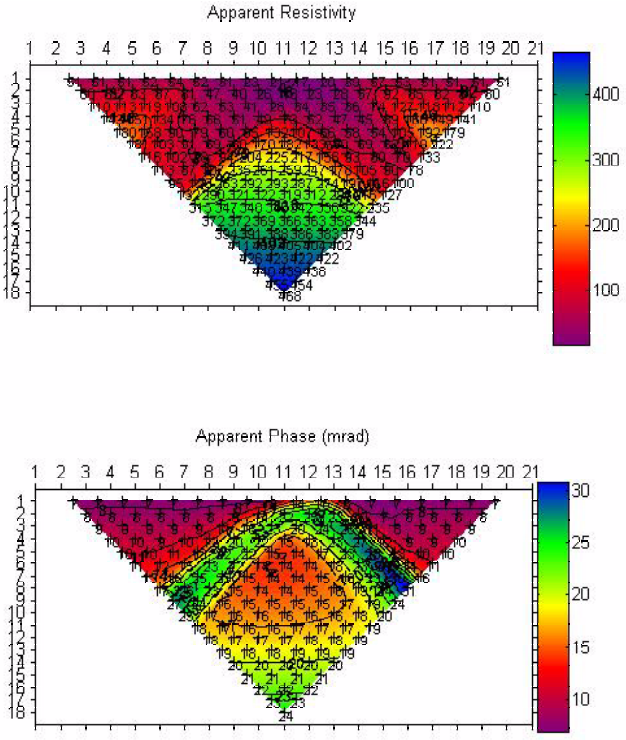

Figure 4-10 Pseudosections of apparent resistivity and phase for Trench-Williams Model 4.

4.2 Southwest U.S. porphyry model

4.2.1 Overview of forward modeling tools based on the Generalized Effective Medium Theory of the IP effect (GEMTIP)

The development of the Generalized Effective-Medium Theory of the IP effect expands the forward modeling capability of EM methods. This new method allows the spectral behavior of rock conductivity to be predicted based on its composition at the grain-scale. The first step is to construct a simplified model of the rock similar to the example in Figure 3-1. This example has two minerals contained in a matrix. Upon simplification of the rock sample a geologic assessment is conducted for grain types, grain radii, grain eccentricity (ellipsoidal case), and volume percent. Grain conductivity, the surface polarizability coefficient, and the relaxation coefficient must be established by lab measurements for each phase of interest. The effective resistivity of the polarized inhomogeneous medium composed of a matrix with l types of spherical grains is given by equation (4.1):

$$\rho_{ef} = \rho_0 \left\{ 1 + \sum_{l=1}^{N} \left[f_l M_l \left[1 - \frac{1}{1 + (i\omega\tau_l)^{C_l}} \right] \right] \right\}^{-1}, \tag{4.1}$$

where:

$$M_l = 3\frac{\rho_0 - \rho_l}{2\rho_l + \rho_0} \text{ and } \tau_l = \left[\frac{a_l}{2\alpha_0} (2\rho_l + \rho_0) \right]^{1/C_l}. \tag{4.2}$$

The additional capabilities of GEMTIP allow for more accurate forward modeling and could open the door to better mineral discrimination in future.

Two new tools have been developed to use GEMTIP. The first is a standalone code to predict the spectral response of a given rock sample. The second tool is the incorporation of GEMTIP as an option for the forward modeling code INTEM3DIP. Four conductivity options are available for use in INTEM3DIP: direct current (DC), conductivity and phase (constant IP across all frequencies), Cole Cole, and GEMTIP models.

4.2.2 Application of GEMTIP to the southwest U.S. porphyry model

We have applied GEMTIP to conduct forward modeling of porphyry ore deposit rocks. Porphyry systems are important geologic targets for mineral exploration. Copper, gold, and molybdenum are among the important minerals extracted from these deposits. Many porphyry systems remain to be discovered and quantified. For this reason the development of a simplified porphyry model

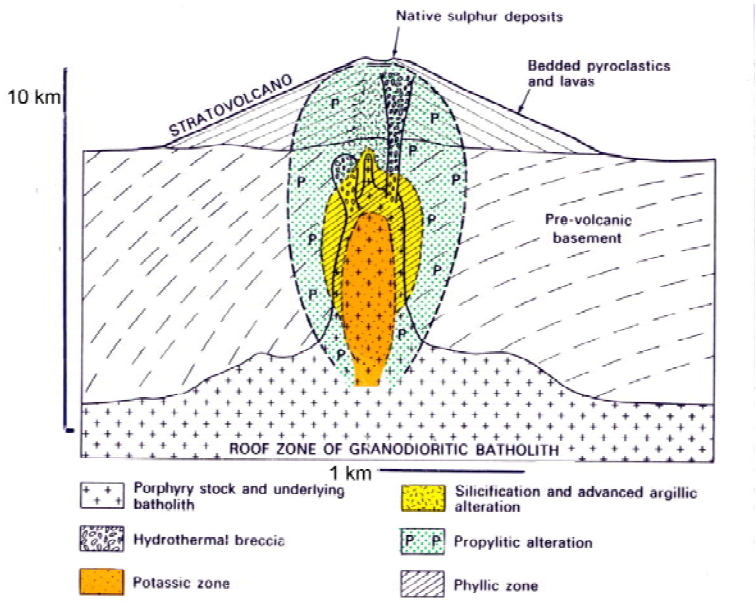

Figure 4-11 A schematic illustration of the creation of a porphyry deposit (after Sillitoe, 1973).

was accomplished for future tests of detectability, the effects of nearby geologic structures, and optimal survey design.

For modeling purposes a simplified porphyry model was constructed based on known geologic information (Titley, 1982, and Pierce and Bolm, 1995). An idealized porphyry copper system is shown in Figure 4-11. Circulating hydrothermal fluids help concentrate economic minerals in the alteration zone surrounding the intrusion. Further concentration of minerals can occur from weathering forming the leached cap and enriched zone. Figure 4-12 shows a resistivity/IP model of a "typical" porphyry copper system in the southwestern U. S. (J. Inman, pers. commun.). This model is characterized by potentially strong EM coupling as well as IP effects. The simplified porphyry model, shown in Figure 4-13, incorporates the classic zones seen in many porphyry deposits including supergene zones: leached cap, enriched zone and the unweathered zones: pyrite shell, chalcopyrite (ore zone), and barren core of the intrusion. A normal fault was also included near the deposit. With a better understanding of the deposit-scale of a porphyry system the rock-scale is investigated.

This model is characterized by potentially strong EM coupling as well as IP effects. We performed various modeling experiments to get an insight into the IP responses for this model. We have used the electrical bipole sources in modeling to simulate the conventional IP responses, but, in principle, the INTEM3DIP software makes it possible to investigate the effects of complex resistivity using various types of sources.

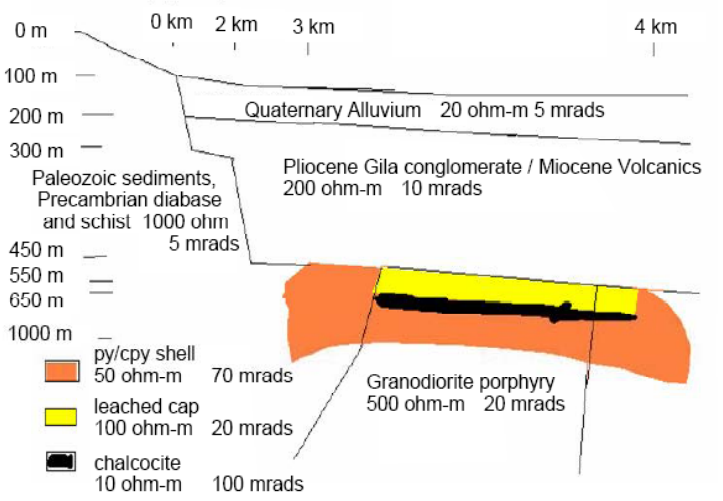

Figure 4-12 Southwest US copper porphyry geophysical model (provided by Joe Inman from Kennecott). It contains basic scale information, geologic units, and geoelectrical properties. Additionally it shows a normal fault on the left side.

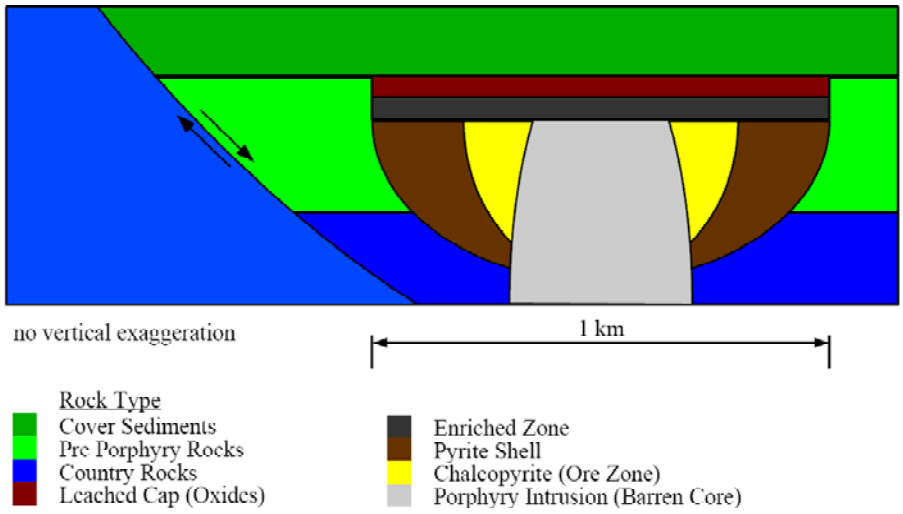

Figure 4-13 A simplified porphyry deposit model. This model incorporates the classic zones of a porphyry deposit and a normal fault.

4.2.3 Rock-scale modeling of porphyry system rocks

Rock-scale modeling is conducted for two porphyry deposit rocks. A comparison of GEMTIP results to Ostrander and Zonge's (1978) empirical data for pyrite and chalcopyrite bearing synthetic rocks is conducted as well. Geologic interpretations of a handful rocks from deposits worldwide were made for this purpose. For their composition two rocks were chosen to be modeled: Bingham chalcopyrite ore and Silver Bell pyrite/chalcopyrite ore. Figure 4-14 shows the disseminated nature of the chalcopyrite grains in a quartz monzonite (QMP) matrix for the Bingham chalcopyrite ore. Disseminated pyrite and chalcopyrite can be clearly seen in the Silver Bell ore in Figure 4-15. The disseminated grains are treated as spheres for the purpose of modeling. A detailed listing of parameters used for forward modeling of the Bingham and Silver Bell ore is provided in Table 2. The behavior of effective resistivity computed by GEMTIP over a broad range of frequencies for the two ores is shown in Figure 4-16. The lower frequency and greater magnitude of the pyrite containing Silver Bell IP response is consistent with the literature (Pelton et al., 1978) although it is known that sulfide type is not the only parameter affecting the IP response (Ostrander and Zonge, 1978).

Table 2

variable	**Bingham**	**Silver Bell**
ρ_{QMP}	200 Ohm-m	200 Ohm-m
$f_{chalcopyrite}$	5	7.5
f_{pyrite}	-	7.5
ω	10^{-2} to 10^{6}	10^{-2} to 10^{6}
$C_{chalcopyrite}$	0.5	0.5
C_{pyrite}	-	0.5
$\rho_{chalcopyrite}$	0.004 Ohm-m	0.004 Ohm-m
ρ_{pyrite}	-	0.3 Ohm-m
$a_{chalcopyrite}$	0.5 mm	0.5 mm
a_{pyrite}	-	0.5 mm
$\tau_{chalcopyrite}$	.0035 s	.0055 s
τ_{pyrite}	-	.03
$\eta_{chalcopyrite}$	0.15 s	0.225 s
η_{pyrite}	-	.224

A comparison has been made of GEMTIP conductivity models with the results of Ostrander and Zonge's 1978 experimental study of chalcopyrite and pyrite bearing synthetic rocks with known matrix resistivities. For Ostrander and Zonge's study rocks bearing either pyrite or chalcopyrite at specific grain sizes were constructed using a cement (matrix) of known resistivity. After the construction of each rock, the frequency of the peak IP response was measured.

Results from this study are plotted as the solid squares and solid triangles in Figure 4-17. The grey shading is used to indicate the range of grain sizes for each measurement of maximum IP response, for example the pyrite synthetic rock plotted at 2.5 mm contains pyrite grains from 2 mm to 3 mm. After a quick experimentation with the values of the surface polarizability coefficient and relaxation coefficient for each mineral type a good correlation between GEMTIP and Ostrander and Zonge (1978) was established (see Figure 4-17). Table 3 gives a detailed overview of modeling parameters used to produce Figure 4-17. These results demonstrate very good correlation between the theoretical GEMTIP curves and experimental data. Note that, application of our knowledge gained on the rock scale will be important for forward modeling and inversion on the deposit scale.

Table 3

Variables	**GEMTIP model**	**Ostrander and Zonge, 1978**
ρ_0 (Ohm-m)	300 Ohm-m	(300 ± 75) Ohm-m
$f_{chalcopyrite}$	5	-
f_{pyrite}	7.5	-
ω (Hz)	10^{-2} to 10^{6} Hz	-
$C_{chalcopyrite}$	0.5	-
C_{pyrite}	0.75	-
$\rho_{chalcopyrite}$ (Ohm-m)	0.004 Ohm-m	-
ρ_{pyrite} (Ohm-m)	0.3 Ohm-m	-
$a_{chalcopyrite}$ (mm)	0.2 - 3 mm	0.2 - 3 mm
a_{pyrite} (mm)	0.2 - 3 mm	0.2 - 3 mm
$\tau_{chalcopyrite}$ (second)	0.001 - 0.28 s	-
τ_{pyrite} (second)	0.02 - 0.87 s	-
$\eta_{chalcopyrite}$	0.15	-
η_{pyrite}	0.15	-

4.2.4 Deposit-scale modeling of a porphyry system

After an investigation of the rock-scale, deposit-scale modeling of a porphyry system is accomplished as well. The developed IE forward modeling code INTEM3DIP is used to conduct the forward modeling. A new interface to allow modeling of geometrically complex geologic systems was developed for the INTEM3DIP forward modeling code. This interface allows the 3D modeling

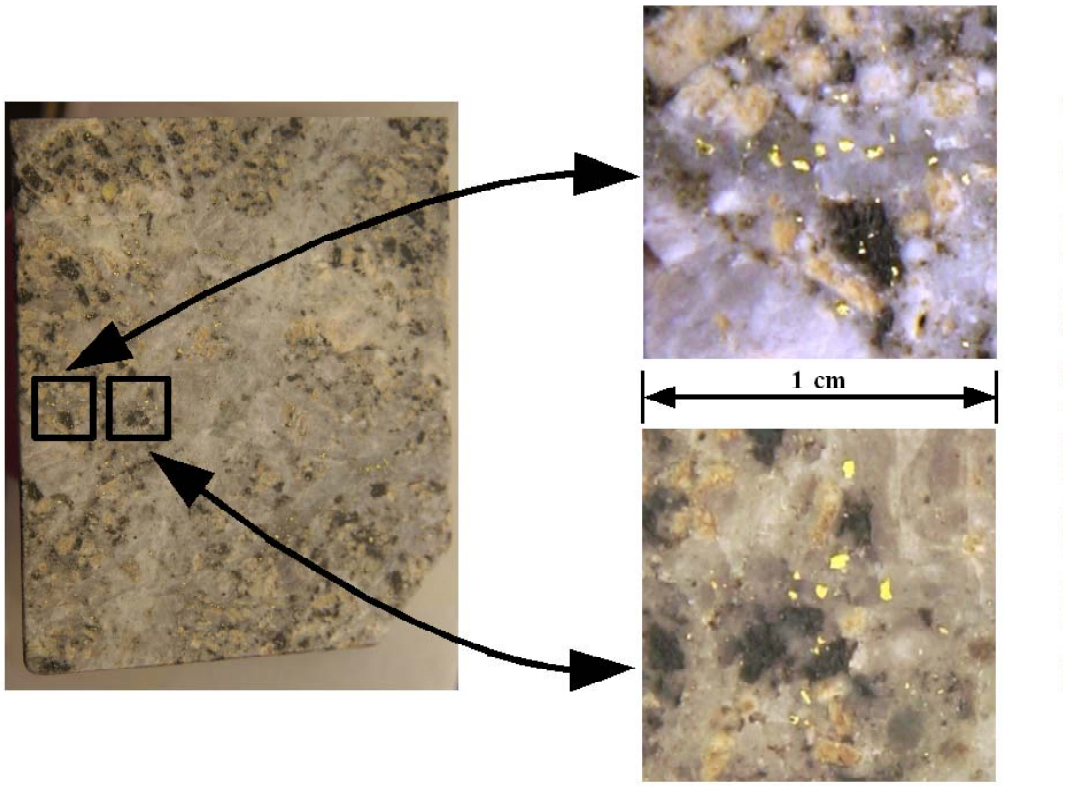

Figure 4-14 Bingham chalcopyrite ore. A core sample of approximately five percent chalcopyrite (yellow mineral) is shown on the left. To better illustrate the disseminated sulfides two one-centimeter crops are shown on the right. This rock would be located in the chalcopyrite zone in the simplified porphyry model.

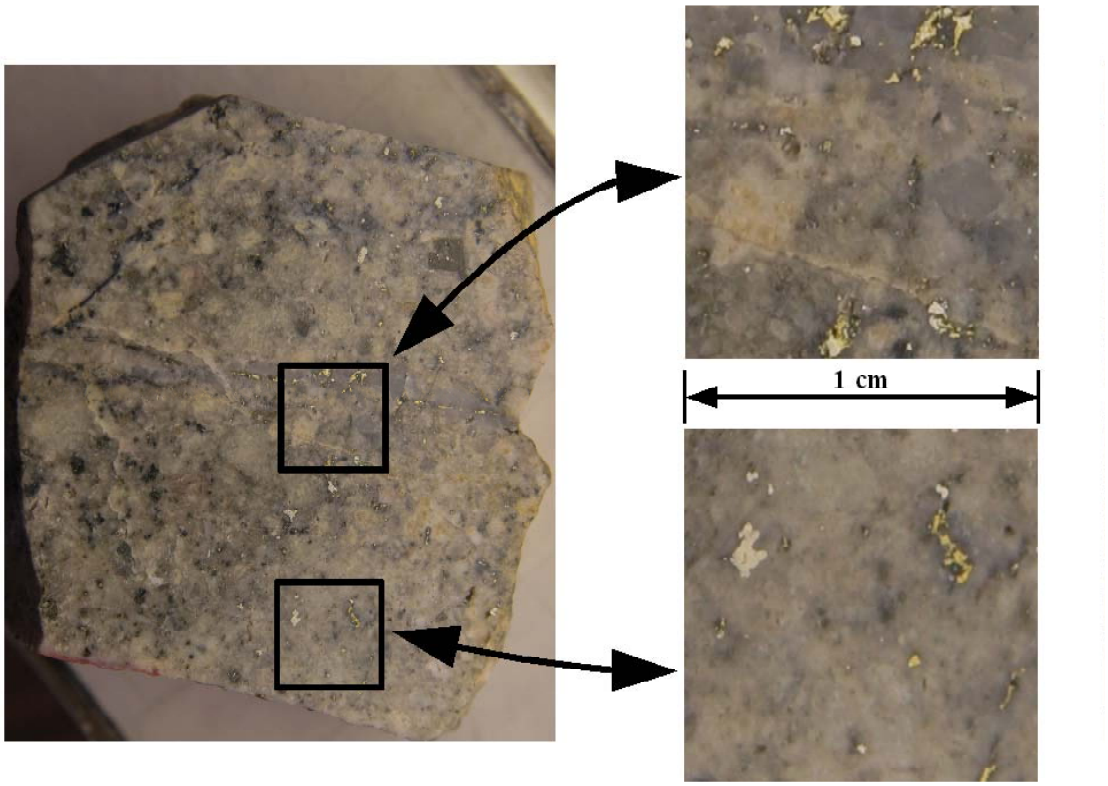

Figure 4-15 Silver Bell ore. This sample contains approximately 7.5 percent chalcopyrite (yellow gold-colored mineral) and 7.5 percent pyrite (pale gold-colored mineral). To better illustrate the disseminated sulfides two one-centimeter crops are shown on the right. This rock would be located between the chalcopyrite and pyrite zones in the simplified porphyry model.

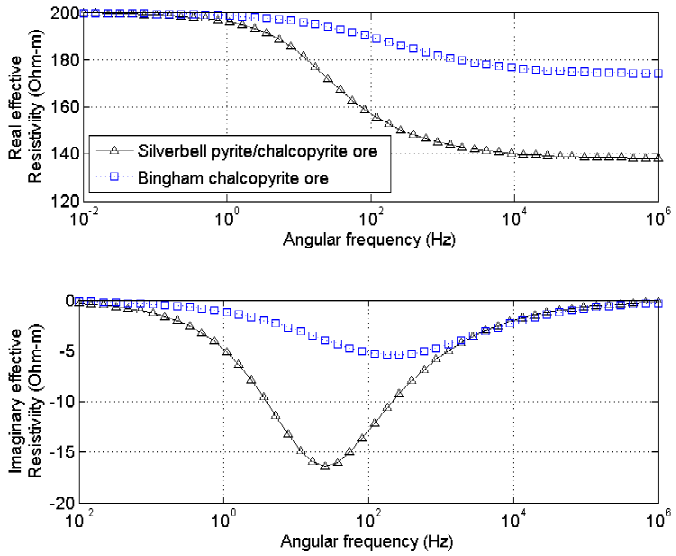

Figure 4-16 Spectral response of Bingham and Silver Bell ores from GEMTIP. Effective resistivity is plotted as a function of frequency for each rock sample.

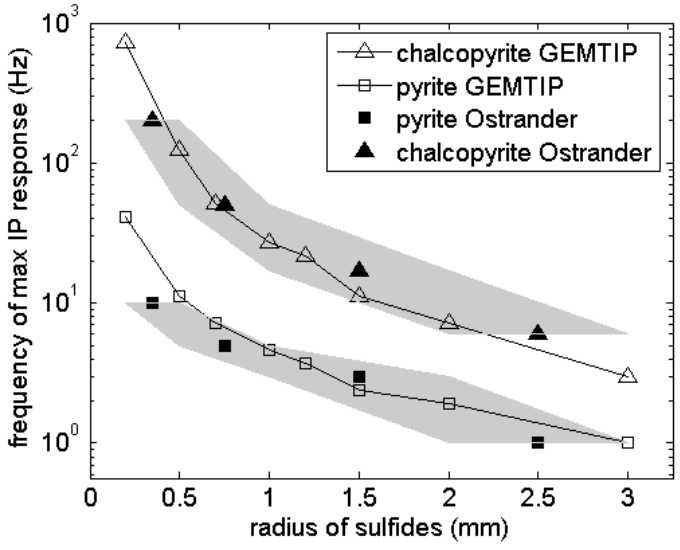

Figure 4-17 Comparison of GEMTIP to empirical data. The results from Ostrander and Zonge (1978) are plotted as filled symbols. The grey shading indicates the range of disseminated sulfide grain size used for each measurement. Results from GEMTIP are plotted using the solid line and open symbols.

of a simplified porphyry model with a nearby fault shown in Figure 4-18. The new interface allows for easy geometric and geoelectric changes to the fault, porphyry deposit, and layered earth background for the study of the effect of these parameters on EM data. The anomalous domain is automatically filled using simple geometric tests. Additionally the discretization is easily changed to allow for more accurate modeling with large discretizations.

A forward modeling was conducted to determine the detectability of the model depicted in Figure 4-18. Table 4 contains a summary of the parameters used to conduct this modeling. The parameters closely follow the SW porphyry model shown in Figure 4-13. The 2000 cell model took approximately 1 hour to run on a standard PC. The clear apparent resistivity anomaly in Figure 4-19 shows the conductive overburden does not hide the 150 meter deep, 80 meter thick, highly conductive enriched zone. The nearby fault produces a slight apparent resistivity anomaly in the left of Figure 4-19. Interestingly and fortunately it does not produce a significant phase anomaly as shown by Figure 4-20. This has important implications for exploration where a DC resistivity anomaly may mask an ore body making the phase response important to the interpretation, indicating the importance of understanding the IP effect of the ore body and surrounding geology.

Table 4

survey type	2-D 200 m dipole dipole
survey length	5000 m
Tx Rx pairs	351
frequencies	0.125, 0.5, 1, 4, 8, and 16 Hz
conductivity model	complex (kcomp = 1)
Anomalous Body	2000 cells
IBC Body	2000 cells
PC Time	1 hour
PC Type	1.4 GHz Athlon, 1 GB RAM

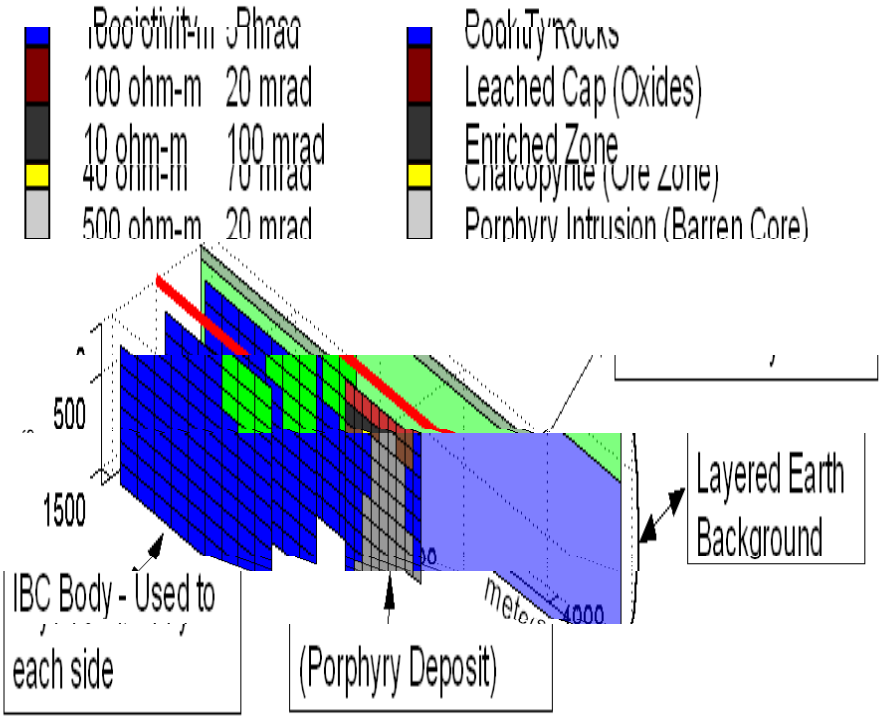

Figure 4-18 MATLAB porphyry forward model. The above diagram depicts the anomalous domain, the location of the survey line, the layered earth background, and the inhomogeneous background for a forward modeling run performed in MATLAB using INTEM3DIP. The enriched zone is 80 meters thick and 150 meters deep.

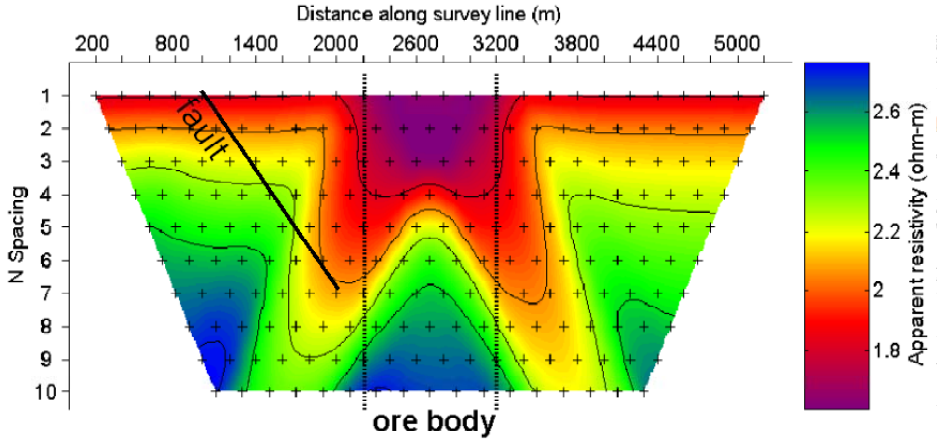

Figure 4-19 Apparent resistivity pseudosection for 1 Hz data. A conductivity anomaly surrounds the ore body in the center. Influence of the fault is seen in the right side of the psuedosection where the apparent resistivity is higher and creates asymmetry in the response produced by the ore body.

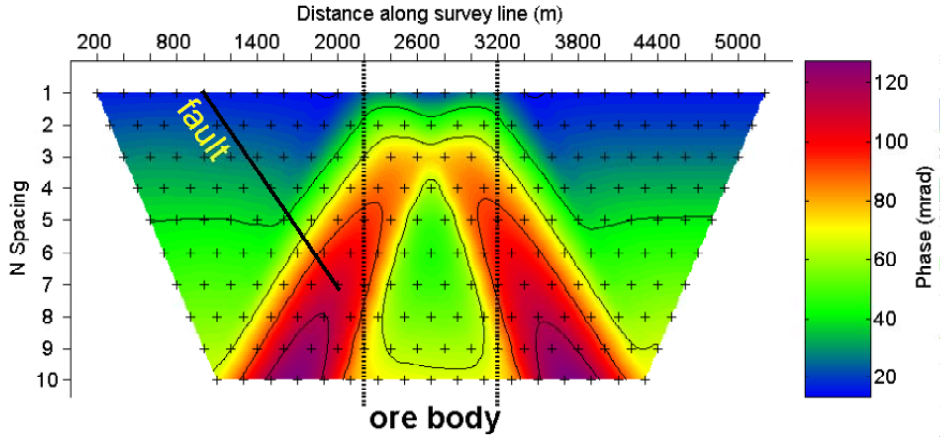

Figure 4-20 Apparent phase pseudosection for 1 Hz data. A phase anomaly due to the ore body is located the center. Influence of the fault is not seen in the phase data as it does not have a strong IP response.

5. RESULTS AND DISCUSSION

During the first two years of the project we have completed the work on Task 1 of PHASE I: construction and analysis of the reliable physical and mathematical models of the IP effect, based on the effective-medium theory. We have developed a new generalized effective-medium theory of multi-phase conductive polarizable media, which provides a quantitative tool for evaluation of the type of mineralization, using the conductivity relaxation model parameters. The geoelectrical parameters of this model are determined by the intrinsic physical and geometrical characteristics of the composite medium: the conductivity contrast between the different phases of the medium and the size and volume of the inclusions (e.g. conductivities and mineral grain or porous sizes). The effective complex conductivity curves produced by this new model may serve as a basis for determining the intrinsic characteristic of the polarizable rock formation from the observed electrical data. These parameters are ultimately used for the discrimination of different rocks, and in this way provide an ability to distinguish between uneconomic mineral deposits and zones of economic mineralization using geophysical remote sensing technology.

We have also completed the work on Task 2 of PHASE I: development of the 3-D EM-IP forward modeling system. We have developed a prototype 3-D EM-IP modeling algorithm and software, based on the contraction integral equation method and generalized minimal residual technique, which improves the convergence rate of the iterative solvers. This software can handle various types of sources and receivers to compute the effect of the complex resistivity model. The development of GEMTIP allows the inclusion of rock-scale parameters such as mineralization and/or fluid content, matrix composition, porosity, anisotropy, and the polarizability of the formations in forward modeling. The 3-D EM-IP forward modeling system includes several conductivity models that may be incorporated: DC, complex resistivity, Cole Cole, and GEMTIP. This allows for more accurate forward modeling of the complex mining targets. We have tested the working version of this code, INTEM3DIP, for computer simulation of the IP data for several models of typical mineral deposits, including a model of a Kambalda-style, nickel sulfide deposit, and a resistivity/IP model of a typical porphyry copper system in the southwestern U. S.

The numerical modeling study helps us to build a foundation for future development of EM-IP modeling and inversion methods, directed at determining simultaneously the electrical conductivity and the intrinsic chargeability distributions, as well as the other parameters of the relaxation model.

6. CONCLUSIONS

The key accomplishments of the first two research years of the project are as follows:

1. A rigorous physical/mathematical theory and model of a multi-phase polarized conductive medium based on the effective-medium approach is developed.

2. The new generalized effective-medium theory of the IP effect (GEMTIP) provides a quantitative tool for evaluation of the type of mineralization, using the conductivity relaxation model parameters.

3. The geoelectrical parameters of the GEMTIP model are determined by the intrinsic physical and geometrical characteristics of the composite medium: the conductivity contrast between the different phases of the medium, the size and the shape of the inclusions, their alignment, and the surface electric polarizability.

4. A new software package for 3-D EM-IP forward modeling has been developed.

5. This new software is able to generate a theoretical EM-IP response for complex 3-D geoelectrical models of mining targets. It can handle various types of sources and receivers to compute the effect of a complex resistivity model.

6. The GEMTIP theory and corresponding forward modeling software are tested for computer simulation of the EM-IP data for several models including a Kambalda-style nickel sulfide deposit and a southwest U.S. porphyry deposit.

7. The numerical modeling study lays a background for future development of the EM-IP inversion method, directed at determining simultaneously the electrical conductivity and the intrinsic chargeability distributions, as well as the other parameters of the relaxation model.

9. A patent application has been filed by the University of Utah: "Geophysical technique for mineral exploration and discrimination based on electromagnetic methods and associated systems."

10. The research papers are in preparation based on the results obtained in the framework of this project.

7. REFERENCES

Bockrih. J., and Reddy. A. K. N., 1973, Modern electrochemistry. Vol. I and II: New York. Plenum Press.

Choi, T.C., 1999, Effective medium theory, principles and applications: Oxford Science Publications, 182 pp.

Cole, K. S., and Cole, R. H., 1941, Dispersion and absorption in dielectrics, J. Chem. Phys., **9**, 343-351.

Davydycheva, S., Rykhlinsky, N., and Legeido, P., 2004, An Electrical prospecting method for oil search using induced polarization effect: 74th Ann. Internat. Mtg., Soc. Expl. Geophys., Expanded Abstracts, Electronic Volume.

Dukhin, S. S., 1971, Dielectric properties of disperse systems: in Surface and colloid science, Vol. **3**: E. Matijevic. Ed., New York, Wiley Interscience.

Hursán, G. and Zhdanov, M. S. , 2002, Contraction integral equation method in 3-D electromagnetic modeling: Radio Science, **37**, 1089,

doi: 10.1029/2001RS002513.

Kamenetsky, F. M., 1997, Transient geo-electromagnetics: GEOS, Moscow, 162 pp.

Kazatchenko, E., Markov, M., and Mousatov, A., 2004, Joint inversion of acoustic and resistivity data for carbonate microstructure evaluation: Petrophysics, **45**, 130-140.

Klein, J. D., Biegler, T., and Hornet, M. D., 1984, Mineral interfacial processes in the method of induced polarization: Geophysics, **49**, 1105-1114.

Kolundzija, B. M., and Djordjevic, A. R., 2002, Electromagnetic modeling of composite metallic and dielectric structures: Artech House, Boston, London.

Komarov, V. A., 1980, Electrical prospecting by induced polarization method: Leningrad, Nedra, 391 pp.

Luo Y., and Zang, G., 1998, Theory and application of spectral induced polarization: Society of Exploration Geophysicists, Tulsa, OK, 171 pp.

Madden. T. R., and Marshall, D. J., 1959. Electrode and membrane polarization: A.E.C. rep. RME-3157.

Marshall, D. J., and Madden, T. R., 1959, Induced polarization, a study of its causes: Geophysics, **24**, 790-816.

McCracken, K. G., Oristaglio, M. L., and Hohmann, G. W., 1986, Minimization of noise in electromagnetic exploration systems: Geophysics, **51**, 819-832.

Mendelson, K. S. and Cohen, M. N., 1982, The effect of grain anisotropy on the electrical properties of isotropic sedimentary rocks: Geophysics, 47, 257-263.

Nelson, P. H., 1997, Induced polarization research at Kennecott, 1965-1977: The Leading Edge, **16**, 29-33.

Norris, A. N., Sheng, P., and Callegari, A. J., 1985, Effective-medium theories for two-phase dielectric media: J. Appl. Physics., **57**, 1990-1996.

Ostrander, A. G., and Zonge, K. L., 1978, Complex Resistivity Measurements of Sulfide-Bearing Synthetic Rocks: 48th Ann. Internat. Mtg., Soc. Expl. Geophys., Expanded Abstracts.

Pelton, W. H., 1977, Interpretation of induced polarization and resistivity data, Ph.D. thesis, University of Utah, 255 pp.

Pelton, W. H., Ward, S. H., Hallof, P. G., Sills, W. R., and P. H. Nelson, 1978, Mineral discrimination and removal of inductive coupling with mulifrequency IP: Geophysics, **43**, 588-609.

Pierce, F. W. and Bolm, J. G , eds., 1995, Porphyry Copper Deposits of the American Cordillera: Arizona Geological Society Digest 20.

Seigel, H. O., 1959, Mathematical formulation and type curves for induced polarization: Geophysics, **24**, 547-565.

Sen, P., Scala, C., Cohen, M. H., 1981, A self-similar model for sedimentary rocks with application to the dielectric constant of fused glass beard: Geophysics, 46, 781-796.

Sheng, P., 1991, Consistent modeling of the electrical and elastic properties of sedimentary rocks: Geophysics, 56, p. 1236-1243.

Sheinman, S. M., 1969, Contemporary physical foundations of the electrical prospecting theory: Nedra, Moscow, 224 pp.

Shuev, R.T., and Johnson, M., 1973, On the phenomenology of electrical relaxation in rocks: Geophysics, **38**, 37-48.

Shwartz, L. M., 1994, Effective medium theory of electrical condition in two-component anisotropic composites: Physica A, 207, 131-136.

Sillitoe, R. H., 1973, The tops and bottoms of Porphyry Copper Deposits: Econ. Geol., **68**, 799-815

Stolz, N., Raiche, A., Sugeng, F., and Macnae, J., 1995, Is full 3-D inversion necessary for interpreting EM data?: Explor. Geophys., **26**, 167-171.

Stone, W. E., and Masterman, E. E., 1998, Kambalda nickel deposits, *in* Berkman, D. A. and Mackenzie, D. H., Eds., Geology of Australian and Papua New Guinean mineral deposits: Aust. Inst. Mining Metallurgy, 347-355.

Stroud, D., 1975, Generalized effective medium approach to the conductivity of an inhomogeneous material: Physical Review B, 12, 3368-3373.

Soven, P. , 1967, Phys. Rev., **156**, 809.

Titley, S. R., ed., 1982, Advances in Geology of the Porphyry Copper, Southwestern North America, University of Arizona Press, Tucson, AZ, 560 p.

Trench, A., and Williams, P. K., 1994, Application of geophysics to nickel sulphide exploration in the Kambalda district, Western Australia, *in* Denith, M. C., Frankcombe, K. F., Ho, S. E., Shepherd, J. M., Groves, D. I., and Trench, A., Eds., Geophysical signatures of Western Australian mineral deposits: Aust. Soc. Explor. Geophys. Special Publication No. 7, 169-179.

Wait, J. R., 1959, The variable-frequency method, in Wait, J.R., Ed., Overvoltage research and geophysical applications: Pergamon, Oxford.

Wait, J. R., 1982, Geo-electromagnetism: Academic Press, New York, 268 pp.

Wong, J., 1979, An electrochemical model of the induced-polarization phenomenon in disseminated sulfide ores: Geophysics, **44**, 1245-1265.

Wong, J., and Strangway, D. W., 1981, Induced polarization in disseminated rocks containing elongated mineralization sulfide ores: Geophysics, **46**, 1258-1268.

Zhdanov, M. S., Dmitriev, V. I., Fang, S., and Hursan, G., 2000, Quasi-analytical approximations and series in electromagnetic modeling, Geophysics, **65**, 1746-1757.

Zhdanov, M. S., 1988, Integral transforms in geophysics: Springer - Verlag, Heidelberg, 367 p.p.

Zhdanov, M. S., 2002, Geophysical inverse theory and regularization problems: Elsevier, Amsterdam, New York, Tokyo, 628 pp.

Zhdanov, M. S., 2005, Development of new geophysical techniques for mineral explorations and mineral discrimination: SME Annual Meeting and Conference, Salt Lake City.

Zonge, K, and J. C. Wynn, 1975, Recent advances and applications in complex resistivity measurements: Geophysics, **40**, 851-864.

Zonge, K. L., 1983, Case Histories of an Electromagnetic Method for Petroleum Exploration: Proprietary Data Sale, Zonge Engineering and Research Organization, Inc.